Earth-Science Reviews 234 (2022) 104199

Contents lists available at ScienceDirect

Earth-Science Reviews

journal homepage: www.elsevier.com/locate/earscirev

Vertical velocity fields along the Eastern Mediterranean coast as revealed by late Holocene sea-level markers

M. Liberatore [a,*], E. Gliozzi [a], P. Cipollari [a], N. Öğretmen [b], G. Spada [c], D. Cosentino [a]

[a] Dipartimento di Scienze, Università degli Studi Roma Tre, Rome, Italy
[b] Department of Ecology and Evolution, Eurasia Institute of Earth Sciences, Istanbul Technical University, Istanbul, Turkey
[c] Dipartimento di Fisica e Astronomia, Università degli Studi di Bologna, Bologna, Italy

ARTICLE INFO

Keywords:
Holocene sea-level markers
Vertical velocity fields
GIA models
Central Anatolian Plateau
Eastern Mediterranean

ABSTRACT

Vertical movements of the solid Earth surface reflect crustal deformation and deep mantle related phenomena. For Holocene times, coastlines displaced from the present mean sea-level are often used together with past relative sea-level (RSL) prediction models to decipher the vertical deformational field.

Along the coastline from southwest Turkey eastward to Israel and Cyprus, field data that constrain Holocene vertical movements are already published, leaving a gap only along the Mediterranean coast of the Central Anatolian Plateau (CAP). Based on new field observations between Alanya and Adana (Mersin, southern Turkey), together with AMS ^{14}C dating, we fill that gap, allowing for the construction of a continuous overview of Holocene vertical differential movements along the Eastern Mediterranean coast. We apply the most recent Glacial Isostatic Adjustment (GIA) models to correct for the glacio-hydro isostatic component of the RSL. Different solutions from the ICE-6G(VM5a) and ICE-7G(VM7) models (developed by W.R. Peltier and co-workers at the Toronto University), and a GIA model developed by K. Lambeck and collaborators at the Australian National University, have been applied to 200 middle-to-late Holocene RSL markers.

Starting from southwest Turkey, we find subsidence between −0.9 mm/yr and − 2.3 mm/yr, corroborating estimates from previous studies. Velocities from the new markers along the CAP Mediterranean coast are positive, ranging between 0.9 and 1.5 mm/yr. These two first blocks are separated by a sharp velocity jump, occurring along the Isparta Angle Fault System one. Such high vertical velocities for the CAP southern margin were predicted by recently published papers that report a rapid uplift phase that peaked during themiddle to late Pleistocene. Moving to the east, velocities are also positive, from 0.2 to 0.6 mm/yr along the coast between the Hatay Gulf and southern Lebanon. The highly variable velocity along the Lebanese sector is likely due to coseismic deformation along the Lebanese Restraining Bend (LRB) faults. To the south, in contrast, the Israeli coast shows stability, according to some unique archaeological RSL markers named piscinae, whereas other markers indicate slow subsidence (−0.2 mm/yr on average). Hence, another velocity jump of at least 0.5 mm/yr is recognizable between Israel and Lebanon. This jump is probably associated with mapped, active tectonic structures. In Northern Cyprus, the only Holocene sea-level marker confirms the near zero vertical velocity values already obtained for the MIS 5e marine terrace. Therefore, a vertical velocity jump occurs between stable Northern Cyprus and the uplifting CAP southern margin, although they occur on the same overriding plate of the Eastern Mediterranean subduction system. High-angle normal faults at the northern margin of the Adana-Cilicia Basin could explain these strongly distinct late Holocene vertical velocity fields.

These results depict a complex framework of independently moving crustal blocks, with kinematic separation along well-known regional fault zones. The drivers of the block movements could be related either to regional tectonics, as it is probably the case for the LRB coast, or to mantle dynamics, such as for the uplifting Turkish sector, where deeper processes should be considered.

* Corresponding author.
E-mail address: marco.liberatore@uniroma3.it (M. Liberatore).

https://doi.org/10.1016/j.earscirev.2022.104199
Received 15 March 2022; Received in revised form 22 June 2022; Accepted 26 September 2022
Available online 7 October 2022

1. Introduction

Vertical displacement of the ground is a common phenomenon of the Earth's surface, driven by both local and regional processes. Few methods are generally used to assess the vertical displacement of a certain area, depending on the phenomenon one is investigating and the availability of data and instruments. GNSS (Global Navigation Satellite Systems) data is commonly used for this purpose, but because the uncertainty of the vertical component (≈1 mm/yr) is commonly in the same range of the tectonic regional velocity field, such data are only useful when the time-series are long enough to substantially reduce uncertainties (tens of years) or when the vertical velocity is well above 1 mm/yr (Johansson et al., 2002; Bennett and Hreinsdóttir, 2007). InSAR (Interferometric Synthetic Aperture Radar) data are satellite images where the elevation of the same place is recorded at different times. If many images are available, it is possible to reconstruct how the ground position changed through time. Like GNSS data, the range of uncertainty is ≈1 mm/yr, so that InSAR data are often used exclusively for investigating faster, recent vertical displacements, such as co-seismic deformation (e.g., Simons et al., 2002). Leveling lines are paths where distances and angles between some reference points are measured at specific time intervals. In some places, these measurements are available over very long-time intervals (one hundred years) and provide high-quality data with which to infer vertical movements of the ground (e.g., Giménez et al., 1996; Spampinato et al., 2013).

Although all these methods are useful, they give insights over a limited time window, of 100 years or less. Potential biases can occur if these geologically instantaneous measurements are assumed to represent the long-term vertical velocity deformation field. In coastal areas, the study of fossil paleo-coastlines offer a powerful alternative to assess long-term vertical velocity fields on a regional scale, as they typically enable time-averaged estimates spanning several thousands of years (e.g., Pirazzoli et al., 1994; Dickinson, 2000; Antonioli et al., 2006; Mourtzas et al., 2016).

The Eastern Mediterranean coast belongs to the western part of the complex system of collision between three main tectonic plates: Eurasia, Arabia, and Africa (Fig. 1). Different tectonic regimes are recognizable in different sectors of the system. Oceanic lithosphere of the Eastern Mediterranean is subducting under the Cyprus Arc, and it is kinematically separated from the Arabian plate to the east, for which continental collision with Eurasia started at 17.5 to 20 Ma (Ballato et al., 2011). Separation between Africa and Arabia occurs along the Levantine Fault System (comprising the Dead-Sea Fault), a transcurrent fault zone made by several segments of left-slip faults separated by restraining bends, releasing bends, and pull-apart basins. All of these fault systems accommodate both horizontal and vertical movements. The geodynamic context of the study area is also complex, with uncommonly fast regional uplifts potentially related to upper-mantle processes. Although several authors have suggested an important role for slab break-off in explaining this rapid uplift (Cosentino et al., 2012; Schildgen et al., 2012a, 2012b, 2014; Öğretmen et al., 2018), the details of the geodynamic processes involved are still poorly understood.

The Eastern Anatolian Plateau (EAP) and the Central Anatolian Plateau (CAP) are two regions involved in this phenomenon (Şengör and Kidd, 1979; Cosentino et al., 2012; Schildgen et al., 2012a, 2012b, 2014). Whereas the former is already well-studied (Şengör and Kidd, 1979; Şengör et al., 2003; Barazangi et al., 2006; Göğüş and Pysklywec, 2008), new findings have recently modified what was originally interpreted to be a long-lasting uplift of the southern margin of the CAP (Cosentino et al., 2012). This sector shows uncommonly high vertical velocities, first recognized based on a middle Pleistocene (450 kyr BP) paleo-coastline reported at ≈1500 m a.s.l. (Öğretmen et al., 2018). Details of the spatio-temporal progression of vertical movements in this crustal sector have been recently reconstructed from modeling marine terrace sequences (Racano et al., 2020) and river-profile inversions (Racano et al., 2021). Both these approaches show a bell-shaped velocity curve peaking at ≈200 ka at an uplift rate of 3.8 mm/yr. Predictions from the marine-terrace modeling yield slower Holocene vertical velocities of 1.2 to 1.6 mm/yr (Racano et al., 2020). Consistent range of uplift rates for the last 50 kyr are from river profile inversions at the CAP southern margin (Racano et al., 2021). However, at the time of that study, there was no field evidence corroborating these values.

Along the CAP southern margin, new ^{14}C dated Holocene coastlines are presented here for the first time. Applying the most updated Glacial Isostatic Adjustment (GIA) models, we calculate the vertical tectonic velocity (a component of the vertical velocity due only to tectonics and mantle-related causes) for this sector. We combine these new results with Holocene relative sea-level (RSL) data for the Easternmost

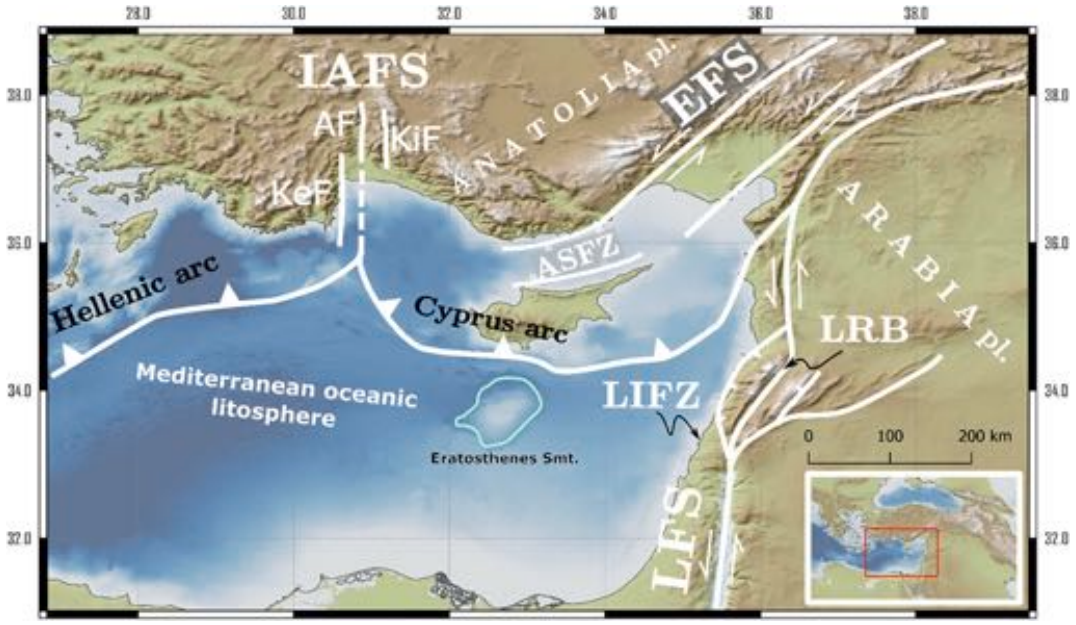

Fig. 1. Synthetic regional sketch in which the main fault systems are reported. pl. is for plate, smt. is for seamount. IAFS - Isparta Angle Fault System; KeF-Kemer Fault; AF-Aksu Fault; KiF-Kirkkavak fault; EFS - Ecemiş Fault System; ASFZ - Anamur/Silifke Fault Zone; LRB - Lebanese Restraining Bend; LIFZ - Lebanon-Israel Fault Zone; LFS - Levant Fault System.

Mediterranean from previously published papers into a single database (see Supplementary Material) and conduct a new analysis of the vertical component using the same GIA models. Comparison of the results gives a picture of what is happening in a complex collision zone, where several different processes, both crustal and sub-crustal, are simultaneously affecting the region.

2. Regional setting

2.1. Vertical velocity field – state of the art

Although good-quality data are available from the literature constraining the vertical velocity field of some individual areas within the Arabo-Anatolian collisional system, a general review of the Eastern Mediterranean vertical velocity field is lacking. In the following, we summarize the currently published data available for the region.

The southern coast of Turkey can be divided into three sectors, from east to west: the Hatay Gulf, the coast along the CAP southern margin, and the western sector of the Antalya District. Dalongeville and Sanlaville (1977) and Kelletat and Kayan (1983) report marine notches and bioconstructed rims higher than the present sea level, but geochronological dating of these features is lacking or is too old to be considered reliable. In the same coastal sector, not far from the city of Alanya, Ciner et al. (2009) report a vermetid reef exposed at 0.5 m a.m.s.l. dated to 1750–1969 cal. yr BP. However, it is not clear whether the isotopic fractionation effect was considered before age calibration, and no local reservoir correction was applied to the final value. In addition, GIA corrections were not applied to these data, with the whole marker elevation considered tectonic in origin. Along the same coastal sector, Ciner et al. (2009) and Desruelles et al. (2009) report four beachrocks at different sites recording sea-levels slightly higher than the present one. However, no dating was performed by the authors on those beachrocks.

Along the coast of southern Turkey west of Antalya, Anzidei et al. (2011) used archaeological evidence from Cnidos, the Gulf of Fethye, and Kekova, after correction with a GIA model, to infer late Holocene subsidence (−0.7 to −1.9 mm/yr) all along the southwest Turkish coast. Negative vertical movements in the same coastal area were previously suggested by Ciner et al. (2009) and Desruelles et al. (2009). These authors report eight beachrocks that are below the present mean sea level, between 0 and − 4.0 m. Two of these beachrocks show ^{14}C ages younger than 2500 cal. yr BP, corroborating late Holocene subsidence for the area.

In the eastern sector of the Turkish coast, within the Hatay Gulf, Pirazzoli et al. (1991) report measurements and dates of emerged wave notches and related bioconstructed rims. Although the same features are discussed in Ciner et al. (2009), no further details are reported. However, in the Hatay Gulf, Ciner et al. (2009) and Desruelles et al. (2009) show three different beachrocks slightly below the present mean sea level. The carbonate cement of one beachrock yields a ^{14}C age of ≈1400 cal. yr BP.

Moving to the south, in Lebanon, the paper by Morhange et al. (2006) represents a key study for the relative sea-level change in the late Holocene based on bio-geomorphological sea-level markers. The same data were used by Elias et al. (2007) and Carton et al. (2009), together with high-quality bathymetric and seismic images, to assess the activity of the Lebanese Restraining Bend.

In Syria, Dalongeville et al. (1993) and Sanlaville et al. (1997) used sea-level markers such as beachrocks and erosional/bioconstructed features to infer relative sea-level changes. However, GIA corrections to remove the isostatic and eustatic components of the vertical velocities were performed only by Sivan et al. (2010), using just one GIA model.

In the Levant, along the coast of Israel, both archaeological and bio-geomorphological data were used to infer relative sea-level changes (Sivan et al., 2001; Sivan et al., 2010; Anzidei et al., 2011; Dean et al., 2019). The large amount of data show overall tectonic stability for the Israeli coast, but some complexities reported in Dean et al. (2019) suggest that further investigation is needed.

2.2. The Mediterranean advantages for RSL markers

The particular climatic and historical conditions of the Eastern Mediterranean make it probably one of the best places in the world to perform analyses on relative sea-level changes. High surface-water temperatures allow subtropical organisms to live all around the coast, leaving constructions and other deposits closely related to the sea-level (Gibson et al., 2006; Morhange and Marriner, 2015). These different features are discussed in detail in section 3.1. Together with these special natural markers, human traces also represent markers for the paleo-sea-level. Ancient settlements, including structures strictly related to sea level along the coast, are spread throughout the Mediterranean area, since historical communities used the sea as the main source for trading, food, war, leisure, and many other activities. Among those structures, salt pans, harbours, coastal villages, and pools once connected to the sea are often used as sea-level markers (Auriemma and Solinas, 2009). All these structures are common since Roman times, but human traces on the coast can also be older in the Eastern Mediterranean, as this coast was one of the first frequented by *Homo sapiens* since 177 ka (Hershkovitz et al., 2018).

But the main advantage of the Mediterranean Sea is probably the low tidal amplitude, on average only about 40 cm (https://www.mareografico.it/?session=0S28652309028774VG90N6871&syslng=ita&sysmen=-1&sysind=-1&syssub=-1&sysfnt=0&code=HOME), due to its limited connection to the Atlantic Ocean. As a result, many of these markers can be tied with relative high precision (±20 cm) to their original sea-level, enabling relative sea-level changes of similar magnitude to be tracked.

3. Materials and methods

The present sea-level leaves many marks of its presence all along coastal areas, including wave notches, beaches, bioconstructions, and human sea-level-based structures. Sea-level markers that are related to past sea levels can reveal important information on the vertical movements of the coastal areas. However, the sea level must be considered as a relative sea level (RSL), which can change either because the ground is moving or the sea-surface is changing, due to polar ice-melting and/or other causes. Therefore, to understand whether the sea surface or the ground moved from its original position, geophysical models of sea-level prediction in the past are used to correct the elevations of paleo-coastlines. Consequently, the age of the sea-level marker, together with its elevation, are parameters that must be known for a paleo-coastline reconstruction. In the Late Holocene, models of sea-level changes, referred to as GIA (Global Isostatic Adjustment) models, are available from the Last Glacial Maximum (LGM) to the present. These models estimate the paleo relative sea-level at a certain age for any location.

GNSS data, InSAR analyses, and leveling lines are unfortunately lacking in the Eastern Mediterranean coast. Instead, we focus our analysis on the relatively abundant sea-level markers. We compile these markers from the Eastern Mediterranean in a database that contains newly collected, unpublished data as well as markers reported in the literature. Newly collected data come from the southern coast of Turkey, between Alanya and Adana, which spans the southern margin of the CAP. Markers from the literature were critically analysed to understand if comparisons among different datasets were possible. As a consequence, some of the markers described in the literature are not included in the new sea-level marker database, because age or other fundamental information are insufficiently clear to be used as reference.

3.1. Compilation of the database

A relative sea-level marker is evidence of an ancient sea level. Its present elevation depends on the relative movements between the sea

level and the ground since the time of its formation.

The most important data needed are the present elevation above or below MSL and the age in addition to the vertical relationship with the paleo sea level (called "functional height" in case of archaeological data) (Hijma et al., 2015; Rovere et al., 2016; Vacchi et al., 2016).

In this study, a database containing 200 markers of ancient coastlines has been compiled from both the literature and newly collected data. The age of each marker was entered into the database after calibration on the most recent curves available. Continental samples were calibrated to the IntCal20 curve (Reimer et al., 2020) while marine samples were calibrated to Marine20 (Heaton et al., 2020). The reservoir effect value is also updated to these curves; using the calib.org tool, we used a delta R value of -142 ± 66. Calibration was performed using https://c14.arch.ox.ac.uk/oxcal.html.

Several types of markers, with different relationships with past sea levels, are included in the database. We consider two macro-groups of sea-level markers: 1) geological markers and 2) archaeological markers.

3.1.1. Geological markers

Geological makers include both bio-geomorphological (e.g., wave-cut platforms, wave notches, trottoirs) and geological, in sensu *strictu*, evidence of ancient coastlines, such as coastal marine deposits, or continental deposits associated with ancient coastlines.

Notches and trottoirs - Wave notches are erosional features carved into the base of a cliff, a few centimetres to several meters deep. Although details of their development are still not clear, many processes take part in it. Their depth, width (from bottom to top), and their evolution through time depend on tidal ranges, bedrock lithology, exposure to wave energy, biological agents, and weathering (Pirazzoli and Evelpidou, 2013; Antonioli et al., 2015; Trenhaile, 2015). Submerged groundwater springs probably also play a role in enhancing the chemical dissolution along carbonate cliffs (Antonioli et al., 2015).

Antonioli et al. (2015) demonstrate the correlation between tidal range and notch width. They show how the notch width is always higher than the mean tidal range, but smaller than the maximum and minimum tidal ranges, whereas the notch vertex corresponds to the MSL. Given the special conditions of the Mediterranean Sea, where the tidal range on average is small (about 40 cm), wave notches are accordingly narrow, making them sensitive trackers for relative sea-level changes.

Encrusting organisms may be associated with the notch, usually forming well-developed semi-continuous rims or patches. Such prominent and well-developed structures are usually referred to as "trottoirs" and they can be associated with a notch or alone, just attached to the cliff. In the Mediterranean, rim-building organisms are coralline rhodophyte *Lithophyllum lichenoides*, brown algae (*Cystoseira* and *Sargassum*), fixed vermetid gastropod mollusks (*Dendropoma*, *Petaloconchus*), barnacles (*Balanus* and *Tetraclita*), as well as *Mytilus* and *Ostrea* (Laborel and Laborel-Deguen, 1996; Antonioli et al., 2015; Rovere et al., 2015).

Some of these organisms live in a very narrow zone around the MSL. A vertical accuracy of ± 10 cm was reported for vermetid rims (*Dendropoma petraeum* species complex, Templado et al., 2016), whereas a vertical accuracy of about 10–20 cm is common for *L. lichenoides* rims. These organisms are often referred to as Fixed Biological Indicators, and they can be used as an independent and reliable relative sea-level indicator (Laborel and Laborel-Deguen, 2005; Schiaparelli et al., 2006).

A notch with its associated rim potentially represents one of the most powerful geological markers, as it provides not only an accurate elevation of the ancient coastline, but also its age, as the suggested Late Holocene rim carbonate material is potentially datable through radiocarbon dating.

Geological markers s.s. - Markers in this group are essentially shallow-marine or continental deposits from which it is possible to determine the vertical relationship with sea level at the time of deposition. These are usually shallow-marine deposits associated with notches or wave-cut platforms, as well as fluvial and alluvial deposits close to the outlets of streams or rivers. Marine breccias or conglomerates are deposits associated with the high energy of a coastal environment, as are beach deposits. Fossils within this kind of sediment can give further information about the paleo-bathymetry as well as their age through radiocarbon dating. Furthermore, deposits related to fossil fluvial plains at the outlet of a river can be used as markers of the base level (MSL).

Among this group of markers, beachrocks represent a unique set of deposits. These are beach deposits affected by fast cementation processes along the infra-littoral zone (just a few years are enough for the rapid cementation of the clasts, as reported in Vousdoukas et al., 2007). Cementation seems to be related to the reactions between fresh phreatic-waters and salt-waters circulating within the sediment. Therefore, under some conditions, beachrocks could be used as a sea-level marker, since they represents a fossil tidal zone (e.g., Mauz et al., 2015a).

3.1.2. Archaeological markers

Archaeological markers are generally those ancient structures associated with human activities, such as fish-tanks, harbour structures, marine pools, and others, for which the functional height and age are known or estimated.

Fish-tanks and other pools - Pools, once connected to the sea, were commonly used by ancient populations for fish breeding or leisure. Features in the pool such as channels and gates allowed the exchange of water with the sea, implying that they had a relationship with the sea level and the tide. Dating could be either from the historical setting or from a datable sample from the structure itself. The best quality data is obtained when both are available and the ages corroborate each other. Datable materials inside these structures could be gastropods (vermetids, patellae), barnacles, or any other organism representing the biological sea level.

Coastal wells - The dataset for Israel mainly consists of ancient coastal wells, which were used for fresh-water supply. The groundwater table in coastal areas (a few hundred meters from the shoreline) is near to the sea level (Dean et al., 2019), because the groundwater table gradient is low, almost zero. Thanks to models and water-level measurements in present-day coastal wells, it is possible to reconstruct the present vertical difference between the water table and the sea level. Once this information is known, it is possible to constrain the ancient sea level from the bottom of a pit (i.e., the only measurement available for fossil pits).

The use of coastal pits as sea-level markers is widely discussed in Sivan et al. (2001) and Dean et al. (2019). Following these papers, a summary can be reported as follows. The groundwater level seasonally changes in relation to aquifer refilling and discharging. A well-built water pit is made deep to enable proper functioning also during the summer, when the groundwater level is at its lowest. But, such a well cannot be too deep, as it may intercept the saltwater table. Given these conditions, this kind of pit should be deep enough to host the entire height of a jar for lifting the water, but the bottom should not be too much deeper than this height to avoid salinization. From archaeological findings, ancient jars used for water capture had a height of ca. 35 cm (± 5 cm). This could be taken as the minimum distance between the bottom of a coastal well and the water table during the dry season. Given the present-day elevation of the bottom of an ancient coastal well, it is possible to obtain the lowest water-table level by adding the jar size. Paleo-sea-level is therefore obtained by subtracting a value (modelled or measured in modern pits) from the paleo-water-table height.

Other archaeological markers - This group of sea-level markers contains sea-level information coming from harbour installations and other coastal structures such as watermills or urban constructions (e.g., Flemming, 1969; Anzidei et al., 2011; Mourtzas et al., 2016; Evelpidou and Karkani, 2018; Dean et al., 2019). Coastal structure floors and basements can be taken as upper constraining points of the sea level at the age of the structure building. Other features that can be considered fully accurate indicators of ancient sea-level come instead from harbours

(Blackmail, 1973). Piers, bollards, and slipways had a particular relationship with the former sea level depending on their age and type, whereas decks and breakwaters can also give some information (Blackmail, 1973; Auriemma and Solinas, 2009).

3.1.3. New geological markers from the southern Anatolia coastal area

New markers of ancient sea level, presented here for the first time, were collected from 2014 to 2016 along the southern Anatolia coastal area, between Alanya and Adana. Much evidence of ancient coastlines higher than the present-day coastline was found along the coast of the CAP southern margin. However, ^{14}C dating has been possible for only a few of them, as many sea-level indicators lack any datable materials. Thanks to these new markers, an almost continuous record of late Holocene coastlines is available for the Near East. This new dataset can fill the gap left from previous studies along the Eastern Mediterranean coast (Pirazzoli et al., 1991; Sanlaville et al., 1997; Sivan et al., 2001; Morhange et al., 2006; Ciner et al., 2009; Anzidei et al., 2011; Dean et al., 2019).

Datings of the markers of ancient coastlines were performed on carbonate material by dating Analytic and CEDAD laboratories through the ^{14}C AMS technique. Conventional ages were corrected for total fractionation effects, and calibration was performed using the 2020 calibration databases (Reimer et al., 2020). A correction of $\Delta R = -142 \pm 66$ accounting for a local reservoir effect is added by using values from the marine reservoir correction database (available as an online resource http://calib.org/marine). This value is the average of eight different estimates available on the eastern Mediterranean coast between Lebanon and Israel (Reimer and McCormac, 2002; Boaretto et al., 2010).

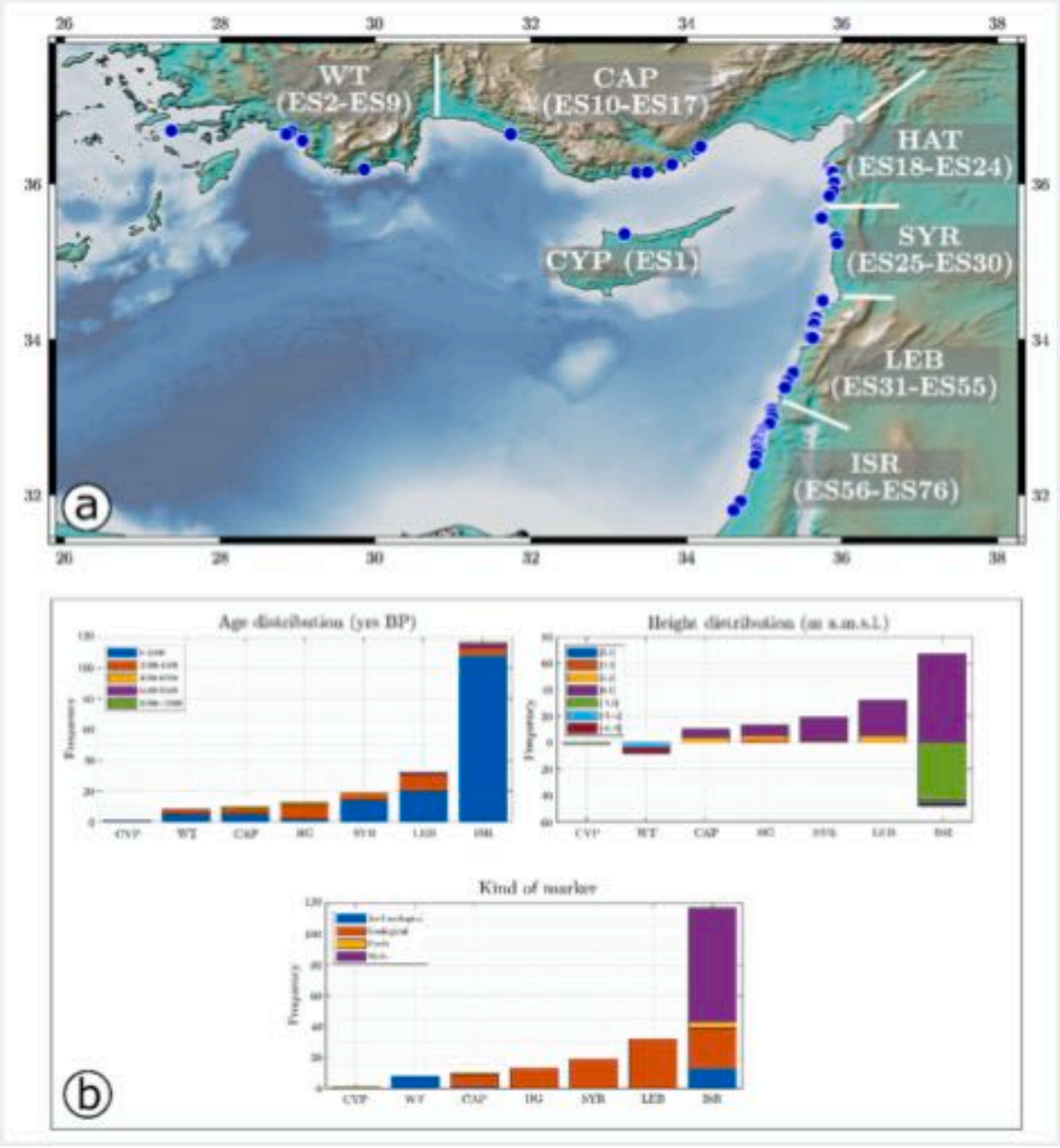

Fig. 2. Structure of the database (EASTMED in supl.mat.). a - In the map the position of the 76 sites (ES1-ES76), comprising a total of 200 sea-level markers is shown (see Sec.3.3 for the definition of "site"). b - Graphs show how the age, elevation and the kind of marker are distributed for each sector of the study area.

3.1.4. Geological and archaeological markers from the literature

The Holocene RSL dynamics along the Near East coast were mostly investigated within the past few decades. Evidence for paleo RSL collected in the new database (Fig. 2) are hereafter described for each sector of the Eastern Mediterranean coastal area (Turkey, Syria, Lebanon, Israel).

3.1.4.1. Turkey – west of antalya. RSL markers from the area west of Antalya are taken from Anzidei et al. (2011), comprising archaeological markers from seven different sites located along the coast of *Fethye Gulf* (between *Knidos* and *Antalya*). These markers can be classified within the group of "*other archaeological markers*". Among them, Anzidei et al. (2011) use harbours, buildings, breakwaters, slipways, and tombs to define the position of the ancient coastlines. The elevation of the sea-level markers is taken with respect to the present sea level by simple optical or mechanical methods during favourable meteorological conditions. These elevations are then corrected for tide and atmospheric pressure to refer the measurement to the current MSL. Ages are estimated based on historical documentation and archaeological data.

3.1.4.2. Turkey – between Antalya and Adana, coastal area of the Central Anatolian Plateau southern margin (CAP coast). A few papers investigated the paleo-sea-level in a quantitative way for this sector of the Anatolian coastal area. Near Incekum, Dalongeville and Sanlaville (1977) and Kelletat and Kayan (1983) report some coastlines 50 ± 20 cm higher than the present sea level. The same coastline is reported and dated by Ciner et al. (2009) at 1859 ± 110 cal. yr BP. This marker is the only one derived from the literature that used in the database for the CAP coast; it corresponds to the "ES10" site.

3.1.4.3. Turkey – east of Adana (Hatay coast). Holocene RSL estimates from this region come from Pirazzoli et al. (1991). As markers of ancient sea-level, they use wave notches and bioconstructed rims, particularly well-developed in this region. Bioconstructions provide datable carbonate material mainly made by vermetids and encrusting calcareous algae. Radiocarbon dating was performed at Paris VI University. Although in the original paper (Pirazzoli et al., 1991) the provided age is reported without the isotopic fractionation correction and calibration (radiocarbon age), Sanlaville et al. (1997) later reported the same dates, adding these two corrections to the original data. Before the age calibration, based on the Stuiver and Reimer (1993) curve, the authors added 400 yr to the original radiocarbon age to account for the reservoir correction instead of the isotopic fractionation, contrary to what is the current accepted protocol. Moreover, this value is similar to the 430 yr often used to correct for fractionation of marine carbonates (Stuiver and Polach, 1977; Price et al., 2002). Therefore, the calibration was performed on a value similar to the conventional age that one could assume for these samples, and the "reservoir correction" reported in Sanlaville et al. (1997) was probably intended as the isotopic fractionation correction. However, it is still unclear whether a local reservoir effect was also considered in the final reported age. However, even if the maximum reservoir age of 350 yr (i.e., the maximum value for the Levant Coast, http://calib.org/marine) were added to the age of each sample, the final vertical velocity would be at most 0.02 to 0.14 mm/yr lower than the values reported in the results section.

3.1.4.4. Syria. Dalongeville et al. (1993) and Sanlaville et al. (1997) dated samples of vermetid bioconstructions from Holocene paleo coastlines in Syria. Radiocarbon dating was performed in the Radiocarbon Laboratory of the Claude-Bernard University in Lyon by liquid scintillation counting. Smaller samples were measured with AMS by the Tandetron machine of the Gif-sur-Yvette Laboratory. Conventional ages are corrected for isotopic fractionation and then calibrated on the Stuiver and Reimer (1993) calibration curve.

3.1.4.5. Lebanon. Morhange et al. (2006) report 32 samples from the Lebanon coast, four of which were previously reported in Sanlaville et al. (1997). Fossil bioconstructions, geomorphological indicators, and beachrocks were used to identify and estimate former sea-level positions. Dated materials comprise vermetids and/or coralline algae coming from bioconstructions, whereas mollusc shells were used for dating the reported beachrocks. The carbonate material was ^{14}C dated at the Laboratoire de Géochronologie de Lyon (France), and the Poznan (Poland) and Groningen (Netherlands) AMS laboratories. Radiocarbon dates from marine specimens were conventionally corrected using ^{13}C measurements and later calibrated on the Stuiver et al. (1998) calibration curve. No local reservoir effects are included in the calculation.

3.1.4.6. Israel. For Israel, the large dataset in Dean et al. (2019) is used together with a few other sea-level markers described in earlier papers. The main dataset is comprised mainly of coastal wells, pools and other archaeological remains built in the antiquity, but also vermetid trottoirs.

Apart from the Dean et al. (2019) dataset, three markers from Anzidei et al. (2011) (at Caesarea and Shiqmona) and four from Sivan et al. (2001) are included in the new database. Those from Sivan et al. (2001) are the oldest, and they could represent an important constraint for the long-term vertical velocity of the Israeli coastal area. Terrestrial organic remains (wood, charcoals, and a mandible) were used for dating. These ages of these markers are reported in the original paper as "uncalibrated age", but it is not cleared whether a correction for isotopic fractionation was performed. Assuming the reported values are conventional ages (corrected for fractionation but not calibrated), we performed calibration using OxCal software (Ramsey, 1995) on the INTCAL20 curve (Reimer et al., 2020). Because the fractionation effect for charcoal and bones is within the range of −55 to +115 yr (Stuiver and Polach, 1977), and the material is relatively old, the lack of a fractionation correction would minimally affect the final ages.

3.2. GIA models used for elevation correction

3.2.1. GIA models – general concepts

The relative sea-level (RSL) is the difference between the local MSL and the local solid surface, the seafloor (Milne et al., 2009; Gregory et al., 2019). As the MSL coincides with the geoid (it is the mean of the sea surface, see Sec.3), the RSL can also be considered as the difference between the geoid and the solid surface at any given location (Gregory et al., 2019). Therefore, RSL can potentially be calculated everywhere, also on the continents. RSL change (ΔRSL) is instead the difference between the present RSL and the RSL at any other point in time. RSL change is due to many processes acting both on the short-term (e.g., waves, tides, atmospheric conditions, and other perturbations) and the long-term (e.g., tectonic displacements, changes of the sea-water volume, isostatic movements, dynamic topography, etc.) (Milne et al., 2009; Khan et al., 2015; Rovere et al., 2016). For this reason, is impossible to understand the cause of a displacement in RSL based on a paleo sea-level marker without an elevation correction that removes some of the components of the RSL. This procedure is commonly carried out for tide-gauge records. A tide-gauge station is frequently equipped with a sea-level sensor and a GNSS device. By removing the ground vertical component from the tide-gauge record, it is possible to isolate the sea-surface fluctuations. (See Fig. 3)

To investigate the tectonic component of a MSL record for the Holocene, it is necessary to correct the marker elevation with a Glacial Isostatic Adjustment (GIA) model. With these models, it is possible to predict the RSL components due to eustasy (E in Eq. (1)), glacio-hydro isostasy (*GHI* in Eq. (1)), and the rotational component (*R*, Eq. (1)) at any point in time. Following a correction that removes these components, the remaining elevation of a sea-level marker is only due to tectonic and deeper components (*T/DC*), Eq. (1)) and some other components that will be defined together as "local components" (*LC*, Eq.

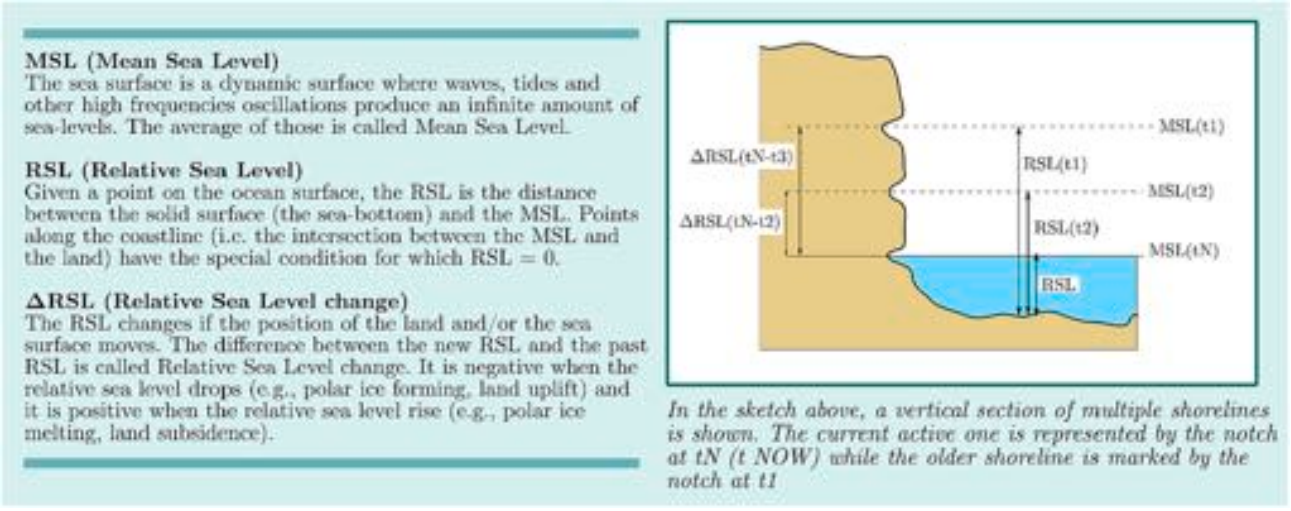

Fig. 3. Terms and concepts of the relative sea level.

(1)). Within this last term are all the mechanisms of vertical land movements mainly due to sediment compaction and/or fluid discharge, either natural or anthropic. These mechanisms can affect the elevation of a marker, but they are not included in the GIA model. That local component can be reduced using markers directly attached to bedrock, so that the sediment-dynamic component can be neglected. However, the local component may include additional components that are not possible to identify or quantify. Included among these components could be, for example, the isostatic signal due to enhanced and long-lasting karst dissolution, which in certain areas should not be underestimated (Rovere et al., 2016). However, in this analysis, the local component is assumed to be small compared with the tectonic one. This assumption is made based on the overall uniformity on a regional scale that is apparent in the results.

The GIA term is intended to encapsulate all the complex dynamics due to mass redistribution, and the related solid earth deformation response, that followed the Pleistocene Last Glacial Maximum (LGM; 26 ka) (Yokoyama et al., 2000; Khan et al., 2015). Since that time, the Earth transitioned from glacial to interglacial climatic conditions, inducing a concurrent global eustatic and isostatic RSL change.

The most prominent GIA signal occurs in the once-glaciated (near-field) regions where ice-unloading induced the well-known phenomena of post-glacial rebound (e.g., Whitehouse, 2018 and references therein). However, GIA effects are known worldwide (e.g., Khan et al., 2015; Rovere et al., 2016). Moving far from the main ice sheets, the ice-induced isostatic signal decreases and becomes comparable to the eustatic one. In these far-field regions, the influx of new water causes a loading effect on oceanic basins, associated with a subsidence signal offshore (Khan et al., 2015). However, due to the short-time response of the lithosphere, the same process induces an uplift signal around continental margins, known as the *continental levering* effect (Mitrovica and Milne, 2002). RSL increases on the continental margins is further enhanced by the effect of ocean siphoning, due to the migration of seawater into the subsiding marine basins (Mitrovica and Milne, 2002; Kopp et al., 2015). As the Mediterranean region belongs to the far-field region (Khan et al., 2015; Mauz et al., 2015b), all these processes play a key role in the non-tectonic Holocene RSL change.

Together with the eustatic-isostatic signal, within the GIA effects, there is a component of the RSL driven by the perturbations to Earth's rotation (*R*, Eq. (1)), due to the global mass redistribution that accompanies GIA. Such effects are evident in the far-field region starting from the mid-Holocene, where the GIA signal is not dominated by the isostatic response, because the eustatic signal becomes negligible.

Eq. (1) sums up the main components of the RSL change following the LGM. Bold letters represent those components predictable through a GIA model.

$$RSL = \boldsymbol{E} + \boldsymbol{GHI} + T/DC + \boldsymbol{R} + LC \quad (1)$$

GIA models are based upon 1) a deglaciation chronology (ice thickness variation in time at a specific location), ii) a rheological profile for the mantle and the lithosphere, and iii) a sea-level equation (see e.g., Spada and Melini, 2019). The viscoelastic structure of the Earth is assumed to be spherically symmetric (i.e., viscosity profile is the same for each earth-radius). A rotational theory is then added to account for the rotational feedback due to the post-glacial mass redistribution.

Large databases that include geological and geophysical observables are used to constrain deglaciation histories. Holocene relative sea-level histories, GNSS and satellite data, and ice-thickness estimations (from exposure-age dating) are among the most commonly used constraints (Peltier and Fairbanks, 2006; Argus et al., 2014; Peltier et al., 2015). A model of the GIA is therefore a combined deglaciation model, viscosity profile, and rotational theory that best fits these constraining data.

3.2.2. GIA models used in this work

Two main families of GIA models are the most commonly used since they are continuously updated and widely tested. These are the ICE-nG models (Peltier, 2004; Peltier et al., 2015; Roy and Peltier, 2018) and the ANU family models (Lambeck and Purcell, 2005; Lambeck et al., 2017). They differ from each other due to different viscosity models or because of the different databases they use to constrain the deglaciation history.

RSL curves used in this work have different sources. Curves with ICE-6G(VM5a) (Peltier et al., 2015) and ICE-7G_NA(VM7) (Roy and Peltier, 2018) come directly from the developers, whereas other curves are obtained using the open-source software SELEN (Spada and Stocchi, 2007; Spada and Melini, 2019). Through the most updated version of SELEN (version 4.0), RSL curves are calculated using the ICE-6G(VM5a) and the ANU model (Lambeck et al., 2017). ICE-6G(VM5a) curves obtained through SELEN are calculated with both a high (HR) and low (LR) resolution setting for the spatial resolution. Given some adaptations made for the deglaciation model ICE-6G in SELEN, final solutions must be considered as the result of a slightly different model from the one of Peltier (Spada and Melini, 2019).

Therefore, we used a total of four GIA models comprising the most updated and globally tested models. Moreover, different resolutions of the SELEN ICE-6G model allow us to test the results of the two different settings. Each model will be described below, while a comparison among the different assumed viscosity profiles shown in Fig. 4.

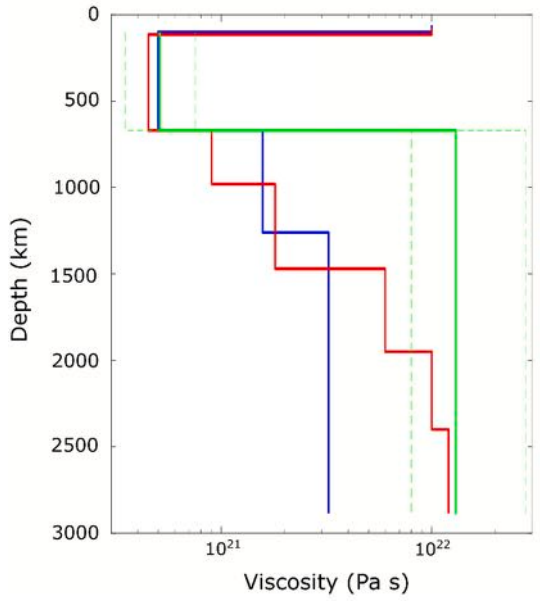

Fig. 4. Comparison of the different viscosity profiles of the GIA models in this paper. VM5a (blue), VM7 (red), and ANU viscosity profile (green – discontinuous line for uncertainty). (For interpretation of the references to colour in this figure legend, the reader is referred to the web version of this article.)

3.2.2.1. ICE-6G_C(VM5a) and ICE-7G_NA(VM7) models from W. R. Peltier. In the models developed by W. R. Peltier, the ICE-nG term indicates the deglaciation history used, while VMy specifies the adopted viscosity profile. The ICE-6G_C model came after the 5G model, integrating both geophysical and geological data from North America, northwest Europe/Eurasia, and Antarctica (Argus et al., 2014; Peltier et al., 2015). The ICE-7G_NA(VM7) model is a later integration of 6G_C, comprising a refinement of the North America component and a different viscosity profile for the lower mantle.

Although these models are based on data far from the Mediterranean area, it has been shown that RSL histories predicted by these models are reliable for the Mediterranean Sea (Roy and Peltier, 2018). RSL markers from tectonically stable areas are particularly powerful for testing a GIA model, as their elevations should be explained only with GIA processes. On this basis, Roy and Peltier (2018) used the extensive database from the western Mediterranean (Vacchi et al., 2016) to demonstrate good fits between Holocene predicted and recorded RSL. These results are encouraging for the application of these two models to correct RSL markers in the eastern Mediterranean as well.

Although the difference between ICE-6G and ICE-7G mainly concerns the Younger-Dryas RSL low at 11 to 12 ka, both models are used in this study, as their curves are different also in the amplitude of the Holocene high-stand. This feature, placed at ca. 5 ka, occurs around the continental borders of the Mediterranean Sea, and it is explainable through the ocean siphoning and continental levering effects. The amplitude of the highstand along the present coastline reaches a maximum within gulfs extending for many kilometers into the continent, as is the case, for instance, of the Iskenderun Gulf hosting the Hatay coast in Turkey. Because the ICE-7G model has a lower highstand peak with respect to the ICE-6G model, the vertical velocities calculated for a marker after correction will depend on which model is chosen.

3.2.2.2. ICE-6G(VM5a) models (LR and HR) from SELEN 4.0. SELEN is one of the few open-source software packages able to calculate RSL curves with specific models of the GIA processes. In the latest version (Spada and Melini, 2019), SELEN 4.0 can calculate RSL curves with two models based on those from the Canadian research group, ICE-5G(VM2) and ICE-6G(VM5a). SELEN predictions are tested both on synthetic and real data. ICE-5G(VM2) is tested on the Western Mediterranean RSL database (Vacchi et al., 2016) whereas ICE-6G(VM5a) is tested on synthetic examples spanning a range of increasing complexity (Martinec et al., 2018).

SELEN solves the sea-level equation (SLE) on a grid with a spatial resolution chosen by the user. High resolution (HR) calculations require powerful hardware to avoid extensive processing times, whereas the low-resolution setting (LR) can be run on normally equipped computers. Both results are considered in this study to evaluate potential differences.

3.2.2.3. ANU model from SELEN 4.0. This model is representative of the other "ANU" group of GIA models (Lambeck and Purcell, 2005; Lambeck et al., 2017). It is different from the ICE-type models with regards to the assumed deglaciation history and the viscosity profiles. ICE-type models consider Antarctic deglaciation ending at about 6000 to 4000 yr B.P. (Argus et al., 2014; Peltier et al., 2015; Roy and Peltier, 2018), whereas ANU models consider that Antarctica ice sheet melting continued later than 4000 yr B.P. (Lambeck et al., 2014). Additionally, the viscosity profile of the ANU models consider a higher and more abrupt viscosity contrast between the lower and the upper mantle compared to ICE-type models (Fig. 4). Finally, ANU models are based on different datasets from the ones of the ICE type, and their codes exploit those datasets differently: in the ICE codes, the focus has been on global solutions, whereas in the ANU models, the focus has been on separate regional solutions (Lambeck et al., 2017).

The ANU model runs on SELEN 4.0 software, but given the extensive hardware requirement, it is not commonly available in the software distribution. Curves with this model are therefore calculated through the geophysical computational laboratory at the INGV institute in Rome.

3.3. Vertical velocity calculation

Correction for GIA is calculated on the coordinate of each marker at its age. Because the age is given with a range of uncertainty, there are three possible GIA corrections: one referred to the central value and the other two referred to the upper and lower limits. The final correction is taken as the mean of the three. This value is then subtracted from the three elevations (central value and its limits), and then vertical velocity is calculated by dividing by the ages. Following standard error propagation, the higher elevation is divided by the lower age and vice versa so that the most distant endmembers are calculated. The vertical velocity for each marker is available in the supplementary material, whereas transects in Section 4.3 show the velocity averaged over *the site*.

The term "site" is intended here with specific meaning. Several markers can refer to the same coordinates, i.e., to the same site. This is possible when several markers lie on the same vertical section, for example, more notches on the same cliff. But more markers can be referred to the same site also because they were originally recorded with low-precision coordinates. The velocity referred to a site is therefore the mean of all the velocities referred to that geographic point. The uncertainty is then the mean of the uncertainties for those markers. We do not report standard error of the mean because the markers are not from the same population. Moreover, it could happen that several markers, with a different relationship with the paleo sea-level (terrestrial/marine boundary, etc.), are referred to the same site. In this case, the site velocity could be "contaminated" by the presence of different types of markers. A site velocity is therefore referred to as *min*, max, or *most probable* velocity based on what kind of markers it contains. A *min* velocity is a kind of site velocity suggesting that the value must be considered as a lower endmember, whereas the *max* site velocity should be considered as an upper endmember. The *most probable* value occurs when all the markers referred to that site represent the exact position of the paleo-MSL. Not all the markers are considered in the transect. Younger markers (those younger than 600 yr B.P.) are excluded because

their elevation uncertainty and the young ages yield very high velocity uncertainties. However, these younger markers, all coming from the Israeli coast, are part of the database, as they still constrain the relative sea level in the elevation uncertainty range.

4. Results

New sea-level markers (both geological and archaeological) from the CAP sector will be presented in this section (Fig. 5). Two beachrocks are also described and dated, but they will be discussed later, together with the data from Ciner et al. (2009) and Desruelles et al. (2009). This kind of marker, as it will be extensively discussed later, show a RSL different from those evaluated with other kinds of markers.

4.1. New late Holocene sea-level markers along the coast of the CAP southern margin

The new RSL markers from the CAP coast are presented from the westernmost to the easternmost sites (Fig. 5).

4.1.1. ES11 – Aydıncık

ES11 comprises sample AYD11 from a 1 m elevated abrasion platform. Fig. 6a shows the relationship between the elevated abrasion platform from which AYD11 was sampled and the currently living trottoir. Fig. 6b shows the sampled calcareous material of AYD11, a marine encrustation mainly made by colonial bryozoa. Even though AYD11 is clearly a shallow marine deposit, the precise relationship with the paleo sea level is not clear. This marker should be therefore considered as a marine limiting point, as it was at or somewhat below the MSL at its formation age.

4.1.2. ES12 – Aydıncık

A section comprising both notches and abrasion platforms at Aydıncık is shown in Fig. 6d. Three samples, AYD4, AYD5, and AYD6, were collected and dated. Their elevations were measured from the current active abrasion platform (MSL) at 0.85, 4.50, 5.50 m, respectively. Dated material comprised a shell of gastropod (*Gibberula miliaria* Linnaeus) for AYD4 and encrusting carbonate for AYD5 and AYD6. However, the origin of the carbonates is uncertain: given the anomalously low ^{13}C content (−11 and − 12 ‰), which is more common for continental carbonates, we consider the ages of these two last samples unreliable. The only reliable sea-level marker is AYD4 (age 4243–44,601 Cal. yr BP), although its relationship with the paleo sea level is unclear. In fact, the sedimentary cap of the abrasion platform, where AYD4 was collected, does not provide a precise reference frame, except that it formed at or under the MSL (most probably 0 to 20 m of depth, according to the Ocean Biodiversity Information System (OBIS) https://obis.org/taxon/139508). This marker should be therefore considered as a marine limiting point, as it was close to but likely below the MSL at its formation age.

4.1.3. ES13 – Yanisli

Yanisli is a small bay opening at the mouth of a river channel. At this location, the RSL information is given by the ancient alluvial plain remains still preserved on the rocky slopes of the bay (Fig. 7). This ancient fluvial-plain section is made by a succession of more or less pedogenized fluvial deposits composed of pebbles in a sandy matrix with large mammal remains.

The ancient fluvial deposits and their related alluvial plain have been temporally constrained by ^{14}C dating of teeth and bones. The elevation of the ancient alluvial plain has been measured with respect to the present-day alluvial plain, which is at the outlet of the Yanisli river channel. Five samples from the top to the base of the ancient alluvial plain deposits and one sample from the present-day alluvial plain deposits were dated. This last age is useful to demonstrate the present-day age of the alluvial plain taken as the counterpart in the elevation measurement of the ancient alluvial plain.

At the base of the ancient alluvial plain deposits, samples YAN1 and YAN2 (bones of *Bos taurus* Linnaeus) yielded ages of 1178–977 cal. yr BP and 1060–930 cal. yr BP, respectively. In the middle of the section, sample YAN3 (a tooth of *Ovis* vel *Capra*) was dated as 923–788 cal. yr BP. Sample YAN5, which is a reworked undetermined marine shell fragment, collected from the top of the section, yielded an older age (1820–1624 cal. yr BP).

4.1.4. ES14 – Egribuk

Within Egribuk Bay, above the present-day active notch, two separate RSL markers are visible (Fig. 8). These are two strips, 10 to 25 cm thick, of marine conglomerate deposits attached to the carbonate rocky cliff at 0.35 and 0.83 m a.m.s.l. The deposits contain marine fossil shells and are laterally continuous for at least 20 m. Mollusc shells supplied carbonate material for dating (samples EGR1 and EGR2). Sample EGR1 was comprised of undetermined mollusc fragments; sample EGR2 consisted of one shell of the gastropod *Columbella rustica* (Linnaeus, 1758), a species most probably living at depths of 0 to 20 m below sea level, according to the Ocean Biodiversity Information System (OBIS) https://obis.org/taxon/139196). Both deposits are related to a shallow marine environment, but their precise location with respect to the paleo sea level is unknown. Thus, these markers should be considered as marine limiting points as they were near, but below the paleo-MSL.

4.1.5. ES15 – Narlıkuyu

East of the village of Narlıkuyu we identified two notches that are higher than the present one (Fig. 9). At the same elevation, a well-cemented breccia containing mollusc remains provided carbonate material for ^{14}C dating. Sample NAR-C1 includes *Thericium* sp. (sent for dating), Columbella rustica (Linnaeus, 1758), unidentified mollusc fragments, Trochidae indet., and a fragment of Pterioida indet. Sample NAR-C2 contains *Truncullariopsis trunculus* (Linnaeus, 1758) (sent for dating), fragments of *Conus mediterraneus* Bruguiere, 1792, and bivalve fragments [*Lima lima* (Linnaeus, 1758) and *Barbatia barbata* (Linnaeus, 1758)]. Although the notches and the deposition of the breccias were likely synchronous, the meaning of these two marine samples in terms of elevation of paleo sea-level needs to be taken with caution, since the marine deposits were deposited at some depth under the MSL.

4.1.6. ES16, ES17 - Ayaş (Elaiussa-Sebaste archaeological site)

Elaiussa-Sebaste, which was part of the old district of *Cilicia Tracheia*, was one of the main trading harbours of the Mediterranean, from the Augustan period (2nd century BCE) until the Byzantine era, with two different harbours: Harbour North and Harbour South. The Arabic invasion that occurred in the second half of the 7th century CE marked its definitive abandonment (Melis et al., 2015). Elaiussa-Sebaste was an important center for oil and wine trading, so its harbours were designed to allow operations of the heavy trading ships, such as the *Navis oneraria* (e.g., Beltrame, 2012).

Melis et al. (2015) report data from a borehole (ELA 6) drilled in the innermost part of Harbour North, to the southwest of the harbour entrance (Fig. 10). Considering the maximum draught of the major ships using the harbour, mainly cargo ships, and the marine palaeodepth reconstruction from the ELA 6 borehole, it is possible to estimate a certain amount of uplift for the Elaiussa-Sebaste Harbour North.

According to the stratigraphy of the ELA 6 borehole (Melis et al., 2015), above the Miocene carbonate bedrock drilled at ca. 13 m depth, a mainly sandy marine succession typifies the sediment core up to ca. 2.5 m depth. Foraminifers, mollusks, and ostracods show shallow-marine environments with several brackish-water events. Above this marine succession, barren gravelly-sand and sand deposits, together with the 0.70 m-thick topsoil, point to a transition to a terrestrial environment (Fig. 10). To date the youngest marine deposits drilled by the ELA 6 borehole, we first obtained the sedimentation rate of the 4 m of sedimentary core, from 7.5 m up to 3.5 m depth, based on ^{14}C dating (Melis

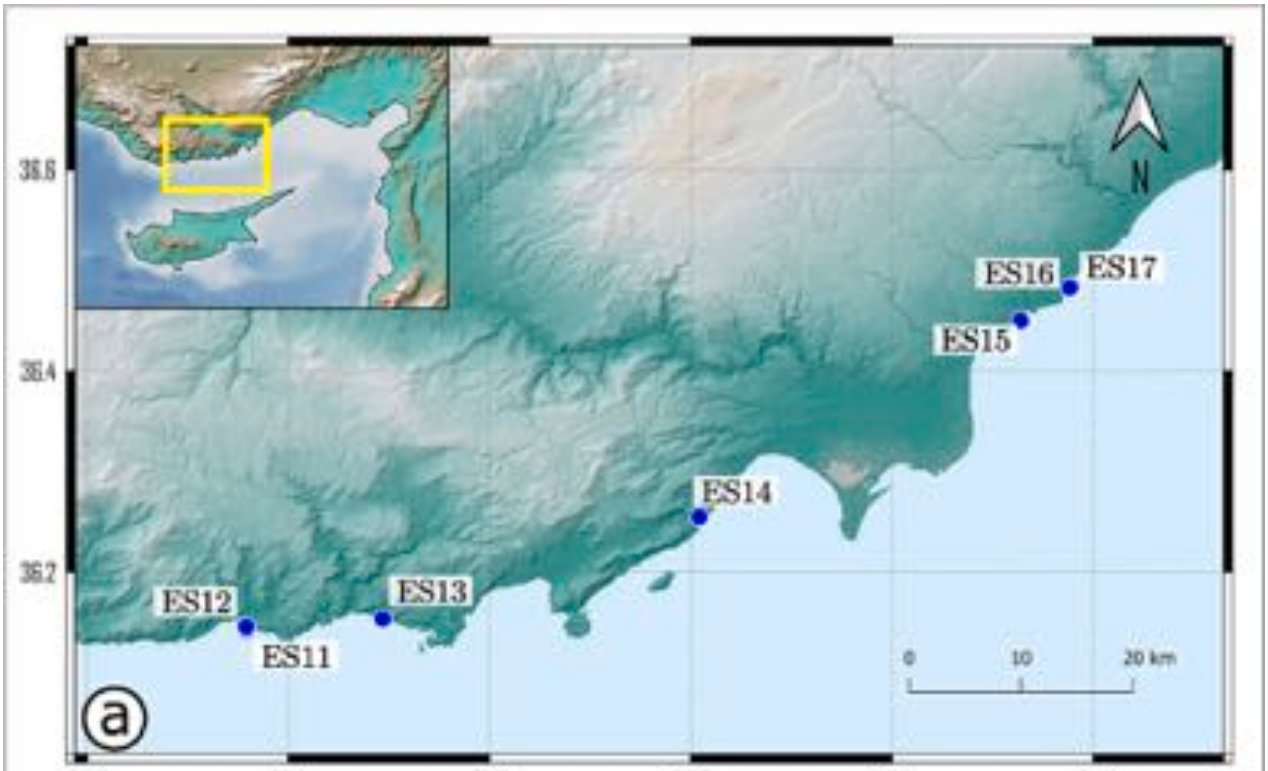

New markers along the CAP southern margin

Site	Marker	Dated material	Conventional age (yr BP)	Age range (2σ cal. yr BP)	Elevation (m)	Kind of marker	Position respect to the paleo sea level	REF
ES11	AYD11	Vermetids encrusting an abrasion platform	1080 ± 30	1136-1309	1.0 ± 0.1	Geological	LL	A
ES12	AYD4	gastropod from a marine breccia (*Gibbula rubens* Linnaeus)	4450 ± 30	4243-4601	0.85 ± 0.05	Geological	LL	A
ES13	YAN	Teeth and bones from a fossil alluvial plain	-	898-1054	1.4 ± 0.3	Geological	SL	A
ES14	EGR1	undetermined mollusc fragment from a marine conglomerate	2470 ± 30	1786-2109	10.35 ± 0.05	Geological	LL	A
	EGR2	gastropod (*Columbella rustica*) from a marine conglomerate	5390 ± 30	5226-5542	83 ± 0.13	Geological	LL	A
ES15	NAR-C1	undetermined mollusc fragment from a marine breccia	2470 ± 30	1786-2109	10.35 ± 0.05	Geological	LL	A
	NAR-C2	gastropod (*Columbella rustica*) from a marine breccia	5390 ± 30	5226-5542	83 ± 0.13	Geological	LL	A
ES16	AYA1	*Patella* sp. from inside an ancient pool from the Roman-Byzantine period	1347 ± 40	614-895	1.2 ± 0.2	Archaeological	SL	A
ES17	ELA	The age comes from three ^{14}C dated charcoal samples retrieved from a borehole in an ancient Roman harbour	-	1365-1665	1.7 ± 0.5	Archaeological	SL	A, B

b

Fig. 5. a) Position of the new markers collected along the coast of the CAP southern margin. b) Data table of the new markers: LL – Lower Level, SL – Sea Level, A – This work, B – Melis et al., 2015.

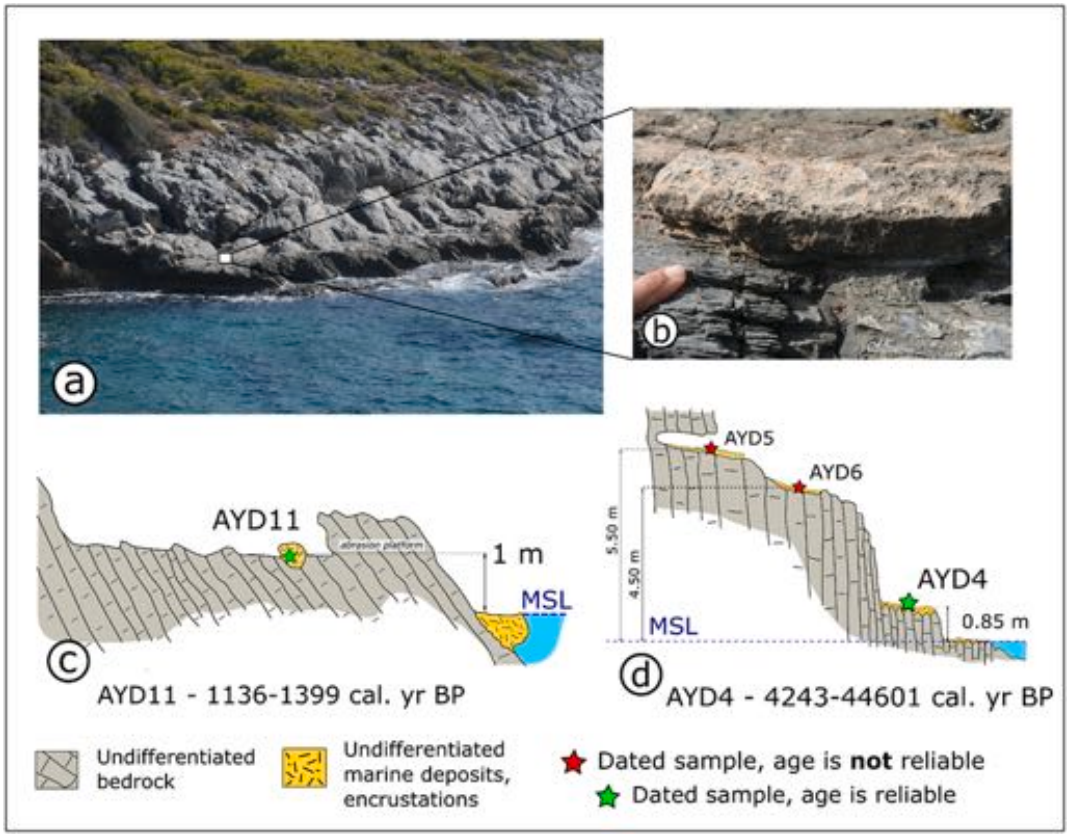

Fig. 6. Markers from the Aydıncık locality. a,c) A raised abrasion platform dated using encrusting deposits on the top of it - b) Detail of the sampled material for AYD11 – d) ES12 - Three raised abrasion platforms are observable, but a source of contamination made the dates of the upper two unreliable.

et al., 2015). The bracketing ages for this interval are 220 ± 93 CE and 392 ± 139 CE, which define a sedimentation rate of 23 ± mm/yr. Consequently, the top of the marine deposits, at 2.5 m below ground level, corresponds to an age of 435 ± 150 CE. Given that the early Byzantine period was characterized by a significant growth in the Cilician economy, with a consequent increase of import and export activities for Elaiussa-Sebaste (Ferrazzoli and Ricci, 2009), its harbours were used until the decline of the city in the 7th century (Melis et al., 2015).

Considering sea-level prediction for that time, RSL in this area was between +11 cm and + 33 cm (depending on the model) higher than the present sea level. Therefore, having the last sea-bottom at −1.3 m with respect to the current MSL, and considering also the GIA signal, the depth of the sea inside the harbour had to be between +1.41 m and + 1.63 m, too shallow to allow ancient commercial ships to get inside the harbour (Fig. 10). These kinds of ships were big enough to move thousands of amphorae full of wine or oil, therefore their draught should have been of a few meters approximately.

The draught for ships entering Elaiussa-Sebaste could be estimated considering the parameters of two end-members of Byzantine ships. Unfortunately, more accurate data are not available, as earlier studies report ship parameters for only a few flat-hulled ships used for river navigation (Auriemma and Solinas, 2009). One endmember is represented by the *Madrague de Giens* shipwreck sunk at around 75–60 BCE. This was probably one of the biggest ships sailing the sea at that time, with a cargo capacity estimated to be >6000 amphorae, or 300 tons. Its draught is estimated to be 3.75 m at full capacity, and 3 m at medium capacity (Bonino, 2018). Another draught estimation comes from the *Yassi Ada* shipwreck found near Bodrum (Turkey) (Van Alfen, 1996). This Byzantine ship, sunk during the 7th century CE, was estimated to have a draught of approximately 2 to 2.5 m (Pappalardo, 2019) although its capacity, 60 tons, was many times less than the *Madrague de Giens*. Based on this information, we estimate that the cargo ships frequenting the Elaiussa-Sebaste harbour should have had a draught similar to the *Yassi Ada* and less than the *Madrague de Giens*. Using a draught of 2.50 m plus 0.5 m accounting for a safety distance between the hull and the sea-bottom, one can estimate a total (tectonic + GIA) 1.7 m of uplift over the last 1365 to 1665 yr.

In the village of Ayaş, within the ancient Roman city of Elaiussa-Sebaste, an important RSL marker was found. The finding is from the northern part of the Elaiussa-Sebaste promontory, close to the remains of the early Byzantine Small Basilica (end of 5th century). The RSL marker is from an ancient pool carved into the Miocene carbonate bedrock, connected to the sea through an original narrow vertical fracture of the limestone (Fig. 11). This pool is equipped with some steps climbing down into the pool, implying that it was probably used for bathing. The present seawater enters now only in the lower part of the pool, with the band of living patellae marking the present MSL. A fossil *Patella* cf. *P. aspera* Röding was found at 1.00 m higher than the living patellae, in a hole carved inside the pool. The fossil *Patella* sp., which was cemented in a sandy matrix, was dated at the CEDAD laboratory. Its age is between 614 and 895 cal. yr BP. As patellids are gastropods living in a short range of elevation around sea level, namely the intertidal zone (Morhange and Marriner, 2015), especially in this case where the pool is protected from the waves, this evidence can be taken as the position of the paleo-MSL. Considering the patellid band to be ≈40 cm thick, as the tidal range in sheltered conditions (https://tudes.harita.gov.tr/), the fossil *Patella* cf. *P. aspera* could be the lowest or the highest *Patella* of the paleo band at that time. If it was the lowest, the elevation of the dated fossil would be 1 m plus 0.4 m a.m.s.l., whereas if it were the highest, its elevation would be 1 m a.m.s.l. In this way, we estimate 1.2 ± 0.2 m of uplift in 755 ± 140 yr.

4.1.7. Beachrocks in Turkey

Along the coast of the CAP southern margin, two beachrocks (BCR9

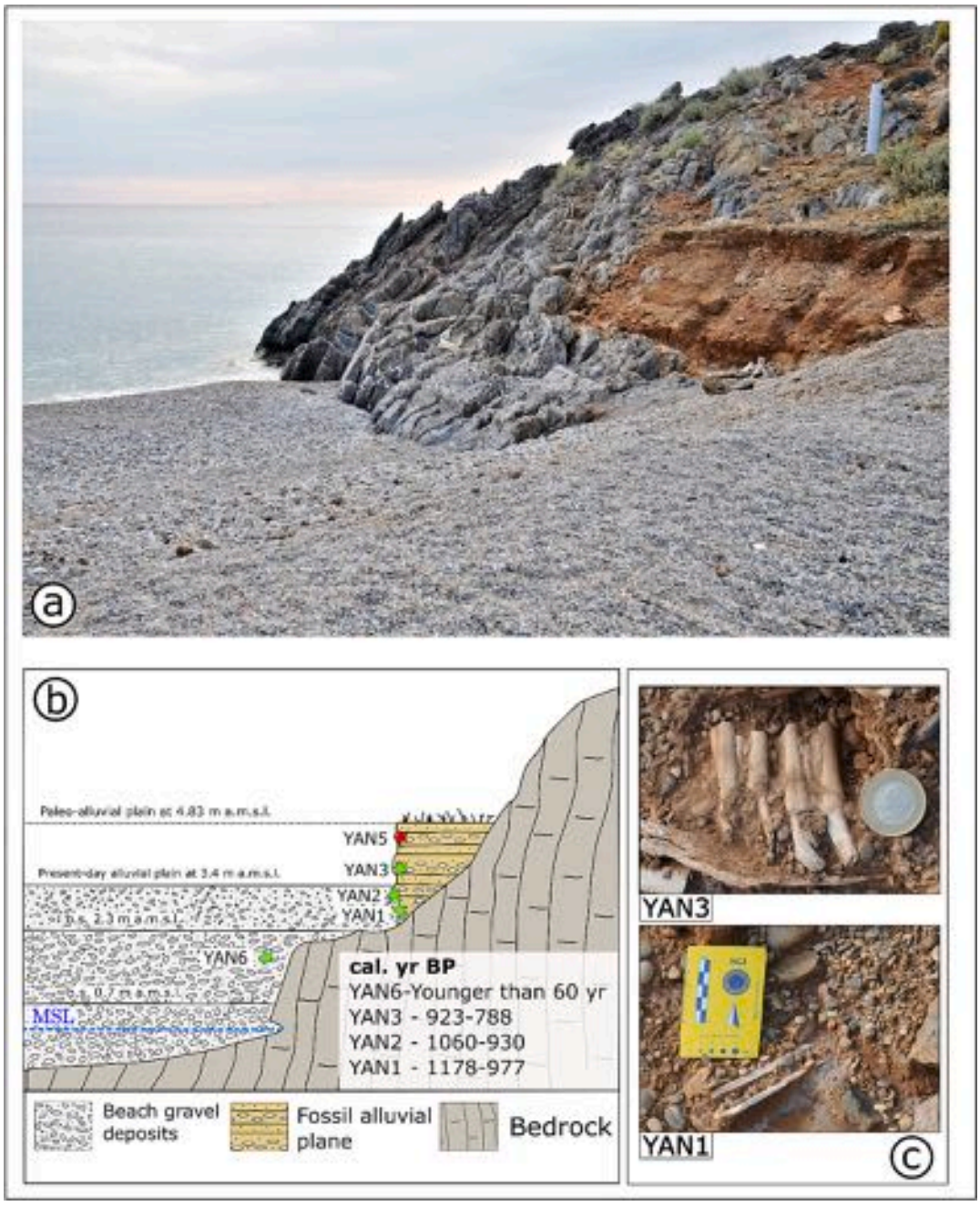

Fig. 7. a) Uplifted and eroded fossil alluvial plain in Yanisli. b) sketch of the sampled section: the age of the paleo alluvial plain is given by the age of large mammal remains (samples YAN 1–3) while the ^{14}C date of a wooden remain (samples YAN6) confirms the present-day age of the berms along the pebbly beach. c) Detail of samples YAN1 and YAN3.

and BCR10.1) were studied during the 2014–2016 field campaigns and dated. These samples are discussed with the other beachrocks from the same coastal sector reported by Desruelles et al. (2009) and Ciner et al. (2009). However, these markers are excluded from the database and the calculation of the vertical velocity field because, as will be discussed later, they describe uplift but with significantly lower velocities than other types of markers. Fig. 12 shows the geographic position and the elevation of each beachrock, while ages and other information are reported in Table 1 and Table 2.

4.1.7.1. Beachrock in Tekeli (BCR9). Along the coast of the CAP southern margin, in the bay of Tekeli, we measured and dated a sandy beachrock that gently dips toward the sea (Fig. 13). The beachrock inland extension is at least 2 m in normal high-tide conditions, but it is certainly wider as, beyond this distance, it is covered by the modern beach. The beachrock maximum elevation reaches 0.32 m a.m.s.l. and remains emerged in normal high-tide conditions. The paleo MSL related to the measured beachrock can be estimated keeping in mind that its highest point was, at the time of its cementation, the mean high tide level. Therefore, using ≈20 cm as the current high-tide mean value above the MSL, is possible to estimate the paleo MSL of the beachrock at 12 cm a.m.s.l. (maximum elevation of 32 cm – 20 cm of mean high tide).

The age of the beachrock comes from a sample of the gastropod *Pirenella conica* (Blainville), taken from the beachrock at ca. 1 m inland of the shoreline (sample TEK1). The age of BCR9, reported as 2σ calibration, is hence 1468 ± 143 cal. yr BP.

4.1.7.2. Beachrock in Aydıncık (BCR10.1). The second beachrock we

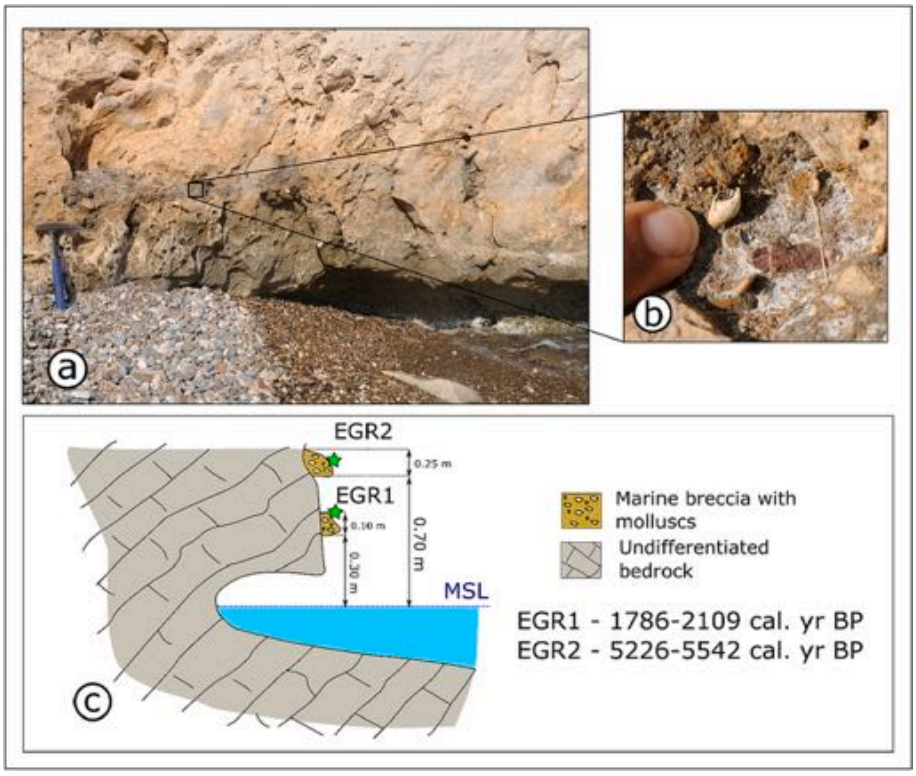

Fig. 8. In the bay of Egribuk (ES14), marine deposits containing shells from marine mollusks are related to two different palaeo sea-levels. 8a shows the marine breccia level from which EGR2 (detail in 8b) was taken. Relation with the two paleosea-levels is shown in 8c.

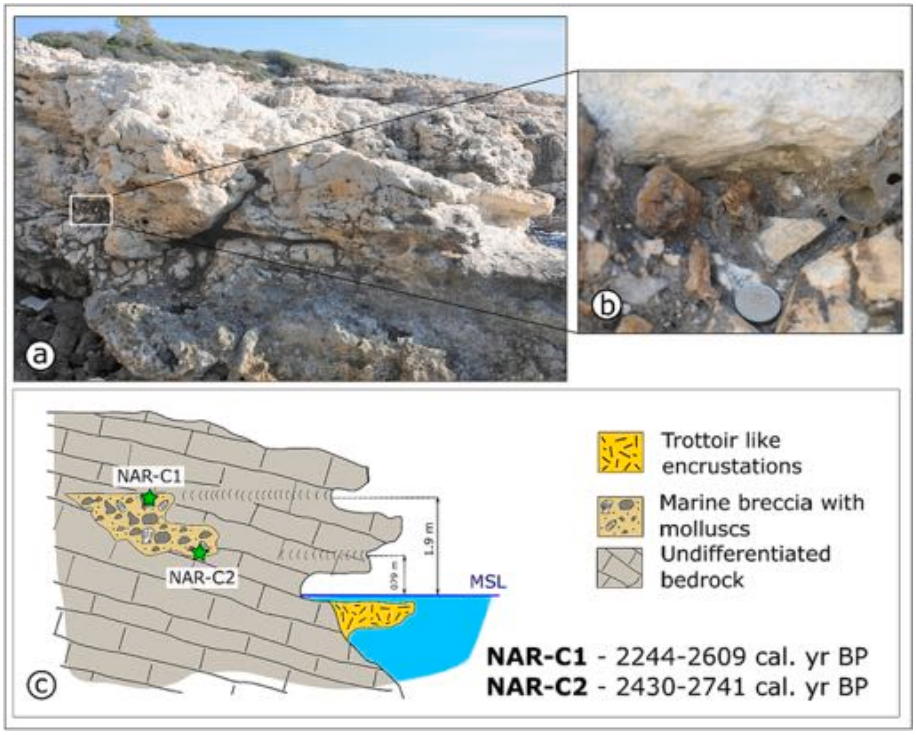

Fig. 9. Along the coast of Narlıkuyu, two different notches are above the present notch. Dated material comes from a marine breccia sampled at the same elevations (NAR-C2 and NAR—C1). a-b) Position and detail of sample NAR-C1e. c) Sketch of the outcrop shows the relative position of the dated samples.

analysed is the same as the beachrock reported by Ciner et al. (2009) and Desruelles et al. (2009), which is site BCR10 in this work. The Aydıncık beachrock is mainly a sandy beachrock, containing coarse sand to conglomeratic cm-thick levels (Fig. 14). It gently deeps toward the sea, but also shows some transverse channels, some meters inland, flooded by seawater. Five datable samples were collected from the BCR10.1 site:

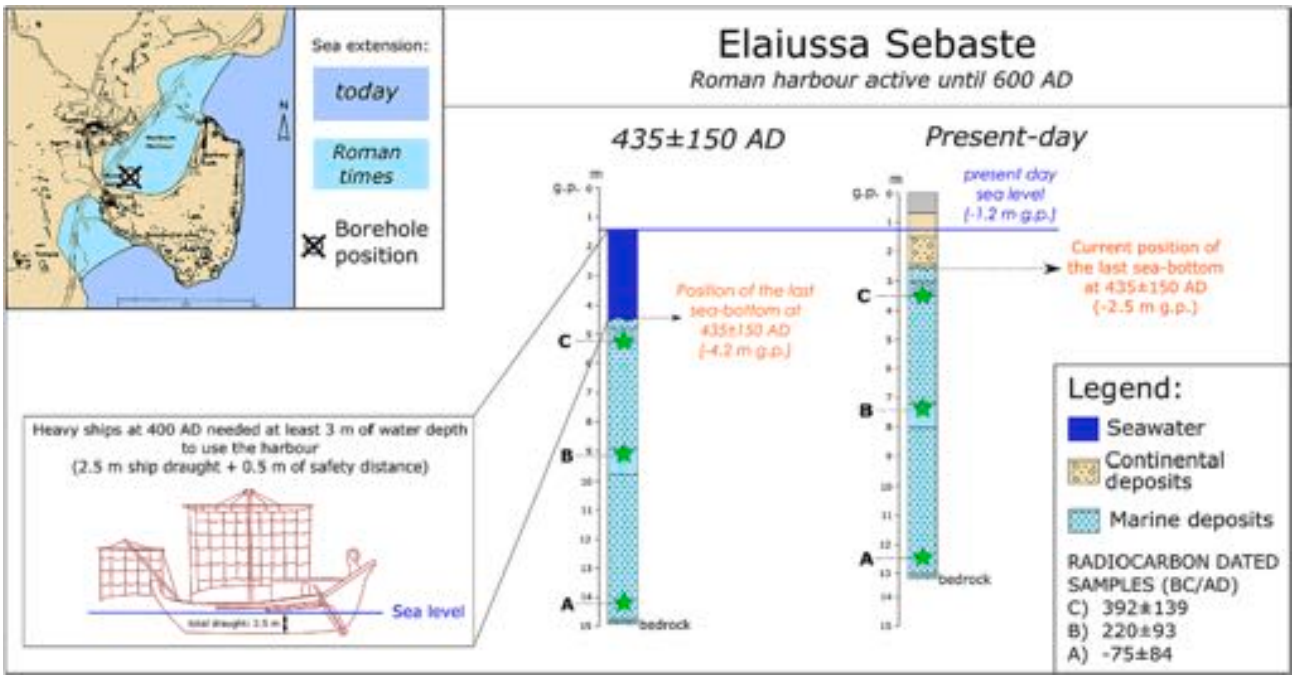

Fig. 10. ELA marker. Borehole data from Melis et al. (2015) allow reconstructing a sea depth within the range 141–163 cm at 430 ± 54 CE. This was too shallow to allow bigger ships (at least 2.5 m draught) to enter the harbour. This paradox can be solved by considering a deeper sea-bottom in the past, prior to tectonic uplift.

AYD7 is a shell fragment of *Thericium* sp. taken at the highest point of the beachrock (0.42 m a.m.s.l.), whereas AYD7a, AYD8, AYD9, and AYD9a are gastropod shells (respectively *Columbella rustica* (Linnaeus), *Gibberula miliaria* (Linnaeus), fragment of *Conus* sp. and fragment of Muricidae gen. sp. indet.) collected from a conglomeratic level of the beachrock. This fossil-rich level remains emerged in normal high-tide conditions at ca. 0.2 m a.m.s.l.

All the ages fall within a close range of mean values between 3200 and 3700 cal. yr BP. The results of the ^{14}C dating of these samples are reported in Table 2. Using the current mean high-tide value of 20 cm, the paleo MSL represented by BCR10.1 is 22 cm a.m.s.l. (maximum elevation of 42 cm – 20 cm of mean high tide).

4.1.8. *Additional evidence for the late Holocene uplift of the coastal area of southern Turkey*

As shown in Fig. 15a, a morphological change in the complexity of the shoreline occurs when passing from the subsiding area west of Antalya to the coastal area to the east. This morphological complexity is shown by the coastal index, which is the ratio between the length of each 25-km long segment and the straight line connecting the two ends. Where the coast is almost straight, the coastal index will be close to 1, whereas for a jagged coast it will be higher than 1. As shown in Fig. 15a, the coastal index shows a marked increase from west to east. This difference could be related to the different vertical velocity fields of the the regions west and east of Antalya, possibly also associated with differing sediment dynamics. To the west of Antalya, subsidence drives the drowning of the drainage system and therefore the sea infills valleys, dividing the coast into narrow gulfs and small islands. In contrast, to the east of Antalya, uplift always keeps the drainage system above the sea level, such that straight structural features are responsible for the coastal morphology. Moreover, prolonged, faster uplift could be associated with a higher availability of sediments, which in turn could be responsible for some leveling and straightening of the coastline. This process could explain why only pocket beaches occur to the west of Antalya, whereas wider and longer ones are observable to the east.

In addition to the previously presented features documenting late Holocene vertical velocities along the southern Turkey shoreline, more potential evidence of subsidence, stability, and uplift are observable. Southwest of Antalya, some Roman remains related to the Phaselis harbour are now submerged (1 in Fig. 15b). In the same area, other submerged structures are reported in Blackmail (1973), as well as in the free online reports from the Akdeniz University (phaselis.org). Even if these features are now underwater, more accurate investigations are needed to understand whether ground subsidence or the normal decay of the site plays the most important role. The 13th century CE shipyard in Alanya (2 in Fig. 15b) shows no evidence of uplift. Moving to the east, some uplifted notches characterize the coast of Yeşılovacık (3 in Fig. 15b), Mavikent (4a in Fig. 15b) and Narlikuyu (5 in Fig. 15b). Moreover, near Mavikent, some outlets of suspended valleys reflect the high uplift rates of the coastal area (4b in Fig. 15b).

4.2. *RSL predictions*

As shown in Fig. 16, GIA model predictions for the Eastern Mediterranean are overall similar, but they differ on a more local scale. Although differences are quite small, not >1 to 1.5 m, it should be considered that this value is of the same order as the elevation of the coastlines in the database. The highstand all along the coastline after 6000 yr BP is a major feature for all the models. As already discussed, it comes from the *ocean siphoning* and *continental levering* effects following a stabilization of the eustatic signal (Mauz et al., 2015b). As shown in Fig. 16, it is similar for each model, but its magnitude in space and time differs between the models. The highstand in ICE-7G (Fig. 16a) is less pronounced both in space and elevation. Major differences are between Peltier's solutions (Fig. 16 a and b) and ICE-6G from SELEN (Fig. 16c). In the latter model, the highstand is higher and wider all along the coast, especially in the narrower Hatay Gulf.

The ANU model (Fig. 16d) yields the same highstand at 5500 yr BP, falling between the 7G (Fig. 16a) and 6G (Fig. 16b) models from Peltier's solutions in terms of spatial extent and magnitude, but the timing is quite different from the ICE-family models. The highstand in the ANU model suddenly starts from 6000 to 5500 yr BP (Fig. 16d), much later than ICE-models, where it starts more gradually before 7000 yr BP (Figs. 16a, b, and c). Moreover, the ANU model's highstand lasts longer than the one from ICE models: at 1000 yr BP, it is more widespread than the other models.

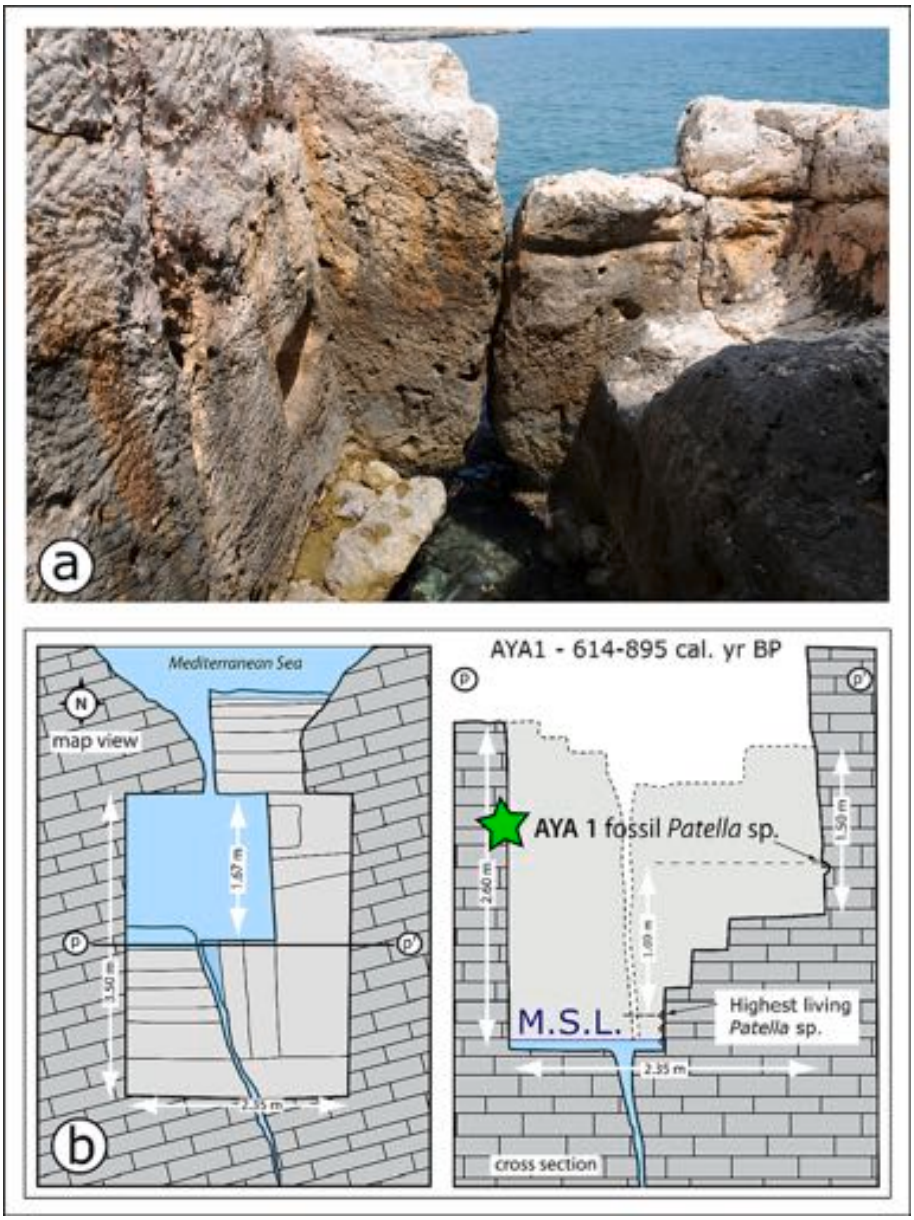

Fig. 11. Marker AYA1 is a Roman pool used for bathing. As shown in the figure, water is now only in the lower part of the pool. a) picture of the inside of the pool; b) sketch of the pool structure, in plan view and cross section.

4.3. Late Holocene vertical velocity fields

The late Holocene vertical velocity field for western Turkey is negative, ranging between −0.9 mm/yr and.

−2.3 mm/yr (WT in Fig. 17a). Moving eastward, the late Holocene vertical velocity suddenly increases to positive values, defining a vertical velocity field that typifies the coastal area of the CAP southern margin with values between 0.9 and 1.5 mm/yr (CAP in Fig. 17a). The first evidence for a positive vertical velocity is found at site ES10 (Suppl. Mat.), even though its vertical velocity value is lower than the eastern ones (ES13, ES16, ES17).

Continuing to the east, another vertical velocity jump to lower velocities is between ES17 and ES18–24, which corresponds to the boundary between the coastal area of the CAP southern margin and the Hatay Gulf. In the Hatay area, the first site (ES18) shows vertical velocities comparable with those along the coast of the CAP southern margin. However, as will be discussed later, we consider the evidence from this site to be unreliable. Vertical velocities remain quite stable between the Hatay Gulf and the southernmost site in Lebanon (0.2–0.6 mm/yr), although many smaller jumps are present between these sites.

One major jump in the vertical velocity field occurs along the political border between Israel and Lebanon. Israel shows small negative values, no more than −0.5 mm/yr, and some sites clearly show stability. One site, which comprises only one sample, is present for Cyprus. Although this sample shows subsidence, it must be considered that it is a fish tank (Lambousa fish tank, Northern Cyprus) built at the MSL and it is still connected with the sea, showing no vertical changes (Galili et al., 2016). Therefore, the vertical velocity computed for this site, although slightly different from zero, is an artefact related to poor fits from the RSL curves. Hence, the vertical velocity for Cyprus is manually adjusted to 0 (green point in Fig. 17b). As shown in Fig. 17b, the late Holocene vertical velocity of Cyprus is lower (≈0 mm/yr) than the sites along the coast of the CAP southern margin, highlighting a vertical velocity jump of at least 1 mm/yr between these vertical velocity fields.

RSL curves for each site, plotted together with the age and the elevation of the related markers, can be seen in the Supplementary

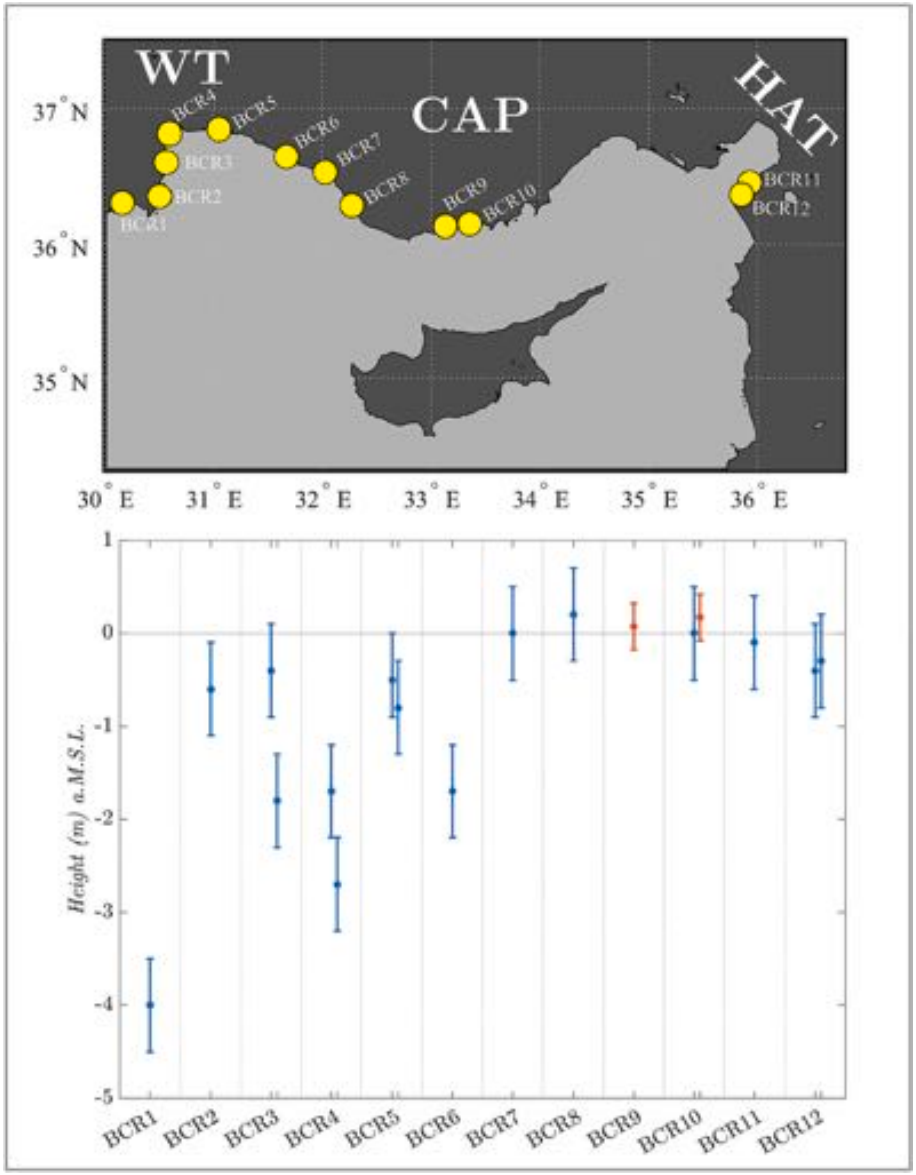

Fig. 12. Position and elevation of the beachrocks along the southern coast of Turkey. Red symbols (with errorbars) refer to the new described and dated beachrocks, whereas blue symbols are data from Desruelles et al. (2009). (For interpretation of the references to colour in this figure legend, the reader is referred to the web version of this article.)

Material. However, some of the RSL curves are shown in detail, for the new dated samples, in the following figures. Fig. 18 shows the RSL curves for the sites along the CAP southern coast. As already mentioned in Sec. 3.1.2, ES10 is the only site with a RSL marker available from literature, whereas sites ES11-ES17 comprise all the newly dated markers. Although the GIA models predict an RSL higher than the current one (due to continental levering and ocean siphoning effects), each marker falls well above the sea-level curve prediction of each model.

Fig. 19 shows the RSL curves compared to the new dated beachrocks and those reported in Desruelles et al. (2009) and Ciner et al. (2009), for which GIA correction was never performed. BCR3 and BCR3.1 are clearly beneath sea-level from all the model predictions. BCR9 and BCR10.1 can be interpreted as stable, whereas BCR11 can be interpreted as a stable or a slightly subsiding marker.

5. Discussion

5.1. Eastern Mediterranean crustal puzzle

Our results suggest that the Eastern Mediterranean coast is composed of adjacent crustal blocks moving with different late Holocene vertical velocity fields. The main velocity jumps occur at the major tectonic discontinuities of the Eastern Mediterranean. Given that the calculated vertical velocity fields are only related to a tectonic component (and/or a local component when the site is not on bedrock), the vertical velocity jumps could be therefore considered as vertical slip-rates along these regional boundary faults.

The main late Holocene vertical velocity jump (difference of 1.8 to 3.7 mm/yr) occurs between western Turkey and the western margin of the CAP (Fig. 17). The coastal area of western Turkey records subsidence with a negative late Holocene vertical velocity of −0.9 to −2.3 mm/yr. This result agrees with what was already found from other authors using different GIA models or methods (e.g., Anzidei et al., 2011; Howell et al., 2017). This region is part of the Western Anatolian Extensional

Table 1
Summary of the beachrocks described along the southern coast of Turkey. In bold are the two new dated beachrocks. 1-New name of the beachrocks' sites; 2-original sample number of the beachrocks reported in Desruelles et al. (2009); 3,4-Geographic coordinates; 5-Middle point of the beachrock (m a.M.S.L.); 6,7-Upper and lower outcrop of the beachrock (m a.M.S.L.), lower values are estimated for BCR9 and BCR10.1 as explained in Sec.4.1.1; 8-Radiocarbon age (cal. yr BP); 9-Locality along the Turkish coast; 10-Bibliographic reference: A-Desruelles et al. (2009), B-Ciner et al. (2009), C-This study.

Beachrocks along the southern coast of Turkey

New ID[1]	Original ID[2] (Desruelles et al., 2009)	LAT[3]	LON[4]	Central Value[5]	Upper Limit[6]	Lower Limit[7]	Age[8]	Locality[9]	REF[10]
BCR1	1	36.309	30.165	−4.0	−3.5	−4.5	n.a.	WT-Finike Bay	A,B
BCR2	2	36.357	30.507	−0.6	−0.1	−1.1	n.a.	WT-Adrasan	A,B
BCR3	3	36.609	30.567	−0.4	0.1	−0.9	1203 ± 145	WT-Kemer	A,B
BCR3.1	3	36.609	30.567	−1.8	−1.3	−2.3	2333 ± 177	WT-Kemer	A,B
BCR4	4	36.818	30.597	−1.7	−1.2	−2.2	n.a.	WT-Kargacik	A,B
BCR4.1	4	36.818	30.597	−2.7	−2.2	−3.2	n.a.	WT-Kargacik	A,B
BCR5	5	36.851	31.050	−0.5	−0.1	−0.9	n.a.	WT-Belek	A,B
BCR5.1	5	36.851	31.050	−0.8	−0.3	−1.3	n.a.	WT-Belek	A,B
BCR6	6	36.651	31.671	−1.7	−1.2	−2.2	n.a.	CAP-Cimtur	A,B
BCR7	10	36.537	31.029	0.0	0.5	−0.5	n.a.	CAP-Alanya	A,B
BCR8	11	36.289	31.275	0.2	0.7	−0.3	n.a.	CAP-Kahyalar	A,B
BCR9	**n.a.**	**36.135**	**31.131**	**0.07**	**0.32**	**−0.18**	1468 ± 143	**CAP-Tekeli**	**C**
BCR10	13	36.153	31.355	0.0	0.5	−0.5	n.a.	CAP-Aydincik	A,B
BCR10.1	**n.a.**	**36.153**	**31.355**	**0.17**	**0.42**	**−0.08**	3318 ± 156	**CAP-Aydincik**	**C**
BCR11	15	36.459	31.931	−0.1	0.4	−0.6	1242 ± 137	HAT-Gozculer	A,B
BCR12	15	36.37	31.854	−0.4	0.1	−0.9	n.a.	HAT-Arsuz	A,B
BCR12.1	15	36.37	31.854	−0.3	0.2	−0.8	n.a.	HAT-Arsuz	A,B

Table 2
- Samples used for dating the beachrocks along the coast of Turkey. In REF coloumn, A is for Desruelles et al. (2009), B is for Ciner et al. (2009), and reference C is this study.

Beachrock datings

Beachrock New ID	Samplename	Dated material	Conventional age (yr BP)	$^{13/12}$C (‰)	Calibration curve	Reservoir effect (ΔR)	Age range (2σ cal. yr BP)	REF
BCR3	Ke2	Cement	1685 ± 30	-4.1	MAR20	−142 ± 66	1230–939	A,B
	Ke3	Internal sediment	1925 ± 35	+4.2	MAR20	−142 ± 66	1466–1178	A,B
BCR3.1	Ke4	Cement	2785 ± 30	+4.4	MAR20	−142 ± 66	2510–2156	A,B
BCR9	TEK1	*Pirenella conica*	2070 ± 30	+0.9	MAR20	−142 ± 66	1611–1325	C
BCR10.1	AYD7	*Thericium* sp.	3710 ± 30	+1.8	MAR20	−142 ± 66	3624–3320	C
	AYD7a	*Columbella rustica* (Linnaeus)	3560 ± 30	+1.6	MAR20	−142 ± 66	3438–3138	C
	AYD8	*Gibberula miliaria* (Linnaeus)	3580 ± 30	+2.4	MAR20	−142 ± 66	3451–3157	C
	AYD9	*Conus* sp.	3830 ± 30	+2.7	MAR20	−142 ± 66	3790–3445	C
	AYD9a	Muricidae gen. sp. indet.	3260 ± 30	+2.3	MAR20	−142 ± 66	3067–2753	C
BCR11	G1	Cement	1774 ± 29	+2.5	MAR20	−142 ± 66	1296–1034	A,B
	G2	Cement	1920 ± 35	+0.4	MAR20	−142 ± 66	1462–1175	A,B

Province, in the western part of the Anatolian microplate (e.g., McKenzie, 1970, 1978; Le Pichon and Angelier, 1979; Jackson and McKenzie, 1984; McClusky et al., 2000; Reilinger et al., 1997, 2006), which includes the Aegean Sea in the western part. Subsidence in this sector is probably related to a combination of the effects of mantle convection and crustal thinning related to extension (Howell et al., 2017).

The CAP southern margin, as already reported, experienced at least two events of uplift (Schildgen et al., 2012a), recently refined as the late Messinian and the middle Pleistocene (Öğretmen et al., 2018; Radeff et al., 2017). Based on both the modeling of marine-terrace sequences (Racano et al., 2020) and river-profile inversions (Racano et al., 2021) in the coastal area of the CAP southern margin, the middle Pleistocene uplift event shows a peak of 3.4 to 3.8 mm/yr at ca. 200 ka. It is worth noting that the Quaternary uplift of the CAP southern margin inferred from modeling of marine terrace sequences estimates an uplift rate of 1.2–1.6 mm/yr for the present day (Racano et al., 2020). Interestingly, these values are close to the vertical velocities estimated in this study based on the uplifted late Holocene shorelines, i.e., 0.9 to 1.5 mm/yr. Hence, the late Holocene uplift of the CAP southern margin could be considered the tail of the middle Pleistocene uplift-pulse recently documented for this area (Öğretmen et al., 2018; Racano et al., 2020, 2021).

The vertical velocity jump between the two areas occurs along with the Isparta Angle Fault System and related faults between Antalya and Alanya (Fig. 17) (e.g., Schildgen et al., 2012b). This fault system is considered to be the linkage between Cyprus and the Hellenic Arc, and it is connected to a slab tearing between the two segments (Glover and Robertson, 1998; Biryol et al., 2011). Although many structural complexities are recognized in this area due to particular stress regimes, the main fault set is oriented NS (Schildgen et al., 2012b; Hall et al., 2014; Över et al., 2016) offering, therefore, a reasonable way also to explain the different vertical velocities. The late Holocene vertical velocity change could be considered transitional in the area between Antalya and Alanya, as the ES10 site shows a transitional vertical velocity (0.17 to 0.35 mm/yr) (Fig. 17) between the positive velocities along the westernmost coast of the CAP southern margin and the subsiding area to the west of Antalya. This transitional zone, with a low vertical velocity, could also explain some archaeological findings near Alanya, showing no appreciable relative sea-level changes. This is the case of the ancient shipyard in Alanya, built during the 13th century CE (Dağgülü, 2009), which shows no signs of uplift (Ciner et al., 2009) (Fig. 15). Assuming the same vertical velocity of ES10 in fact, the 800 yr old shipyard would have been elevated only 14–28 cm, a change too small to be detected.

Vertical velocity jumps also occur between the coastal area of the CAP southern margin and Cyprus, to the south, as well as between the

Fig. 13. Beachrock sampled in Tekeli: sample TEK 1(site BCR9).

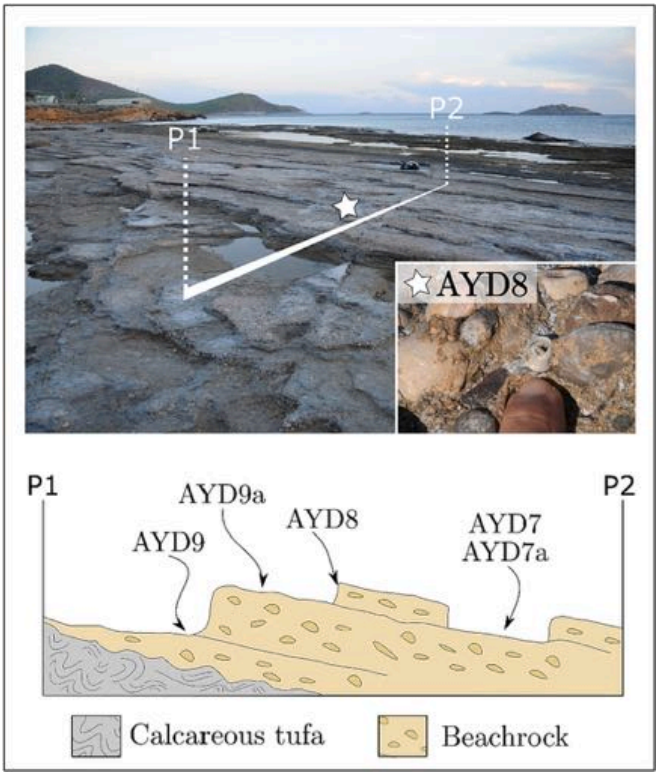

Fig. 14. Beachrock sampled in Aydıncık: samples AYD 7, AYD 7a, AYD 8, AYD 9, AYD 9a (site BCR10.1).

CAP southern margin and the Hatay coast, to the east (Fig. 17). Although for Cyprus only one marker is available (CYP1), its late Holocene vertical velocity (≈0 mm/yr) is in good agreement with a Late Pleistocene vertical velocity of <0.12 mm/yr estimate by Galili et al. (2016) for MIS 5.5 deposits at the northern coast of Cyprus. Therefore, assuming stability for Cyprus, a vertical velocity jump is identifiable between Cyprus and the CAP southern margin (>1.0 mm/yr). Movement between these two crustal blocks could be achieved through slip along the mainly offshore faults at the northern margin of the Adana-Cilicia Basin. As shown by Ozel et al. (2007) and Aksu et al. (2021), offshore the area of Silifke, some high-angle normal faults, dipping toward the basin, are well visible on high-resolution seismic lines, and break both through Holocene marine deposits and the seafloor (Anamur-Silifke fault zone in Aksu et al., 2021) (ASFZ in Fig. 17). These faults are active and capable, and they are associated with a continuous release of seismic energy associated with frequent low magnitude earthquakes (M < 3–3.5, Ozel et al., 2007). Our results suggest that active tectonic discontinuities at the southern margin of the CAP accommodate differential vertical movement of two crustal blocks characterized by differential late Holocene vertical velocities. As already suggested by Ozel et al. (2007), Aksu et al. (2014), and Öğretmen et al. (2015), these tectonic discontinuities, which show late Holocene activity, should be considered part of the Ecemiş Fault Zone, dominated by east-west extension, with a very small component of strike-slip (Jaffey and Robertson, 2001).

Moving eastward toward the Hatay zone, site ES18 includes only the HAT1 late Holocene sea-level marker. This site shows a particularly high vertical velocity if compared with the rest of the Hatay zone (0.2 to 0.8 mm/yr, Suppl. Mat.). The late Holocene vertical velocity of ES18 is similar to those recognized along the coastal area of the CAP southern margin. It is worth noting that this site is tens of kilometers east of the sites referable to the CAP southern margin, whereas it is on the same coastal segment as the other late Holocene sites from the Hatay zone. For this reason, we consider the late Holocene vertical velocity of ES18 unreliable, potentially affected by some errors in defining the age of the sea-level marker.

A fossil rim associated with a notch was used to calculate the vertical velocity for marker ES18 (HAT1 marker). It is ≈3 m higher than the present MSL and gives an age of only ≈2100 yr BP (Pirazzoli et al., 1991; Sanlaville et al., 1997). In the same area, only 4 to 5 km from ES18, another fossil rim (HAT2) at almost the same elevation of HAT1 (ca. 3 m a.m.s.l.) gives an age of ≈4900 yr BP. HAT2 is consistent with the late Holocene vertical velocities obtained from the other sites in the Hatay zone. Given that there are no mapped faults between HAT1 and HAT2, carbon contamination with younger carbon could be a possible explanation for the inconsistent age of HAT1. For this reason, we did not include site ES18 (HAT1) in the analysis of the vertical velocities of the Hatay zone.

The remaining late Holocene vertical velocities in the Hatay zone range from 0 to 0.9 mm/yr, with values mostly between 0.2 and 0.6 mm/yr. Given the higher late Holocene vertical velocity values along the

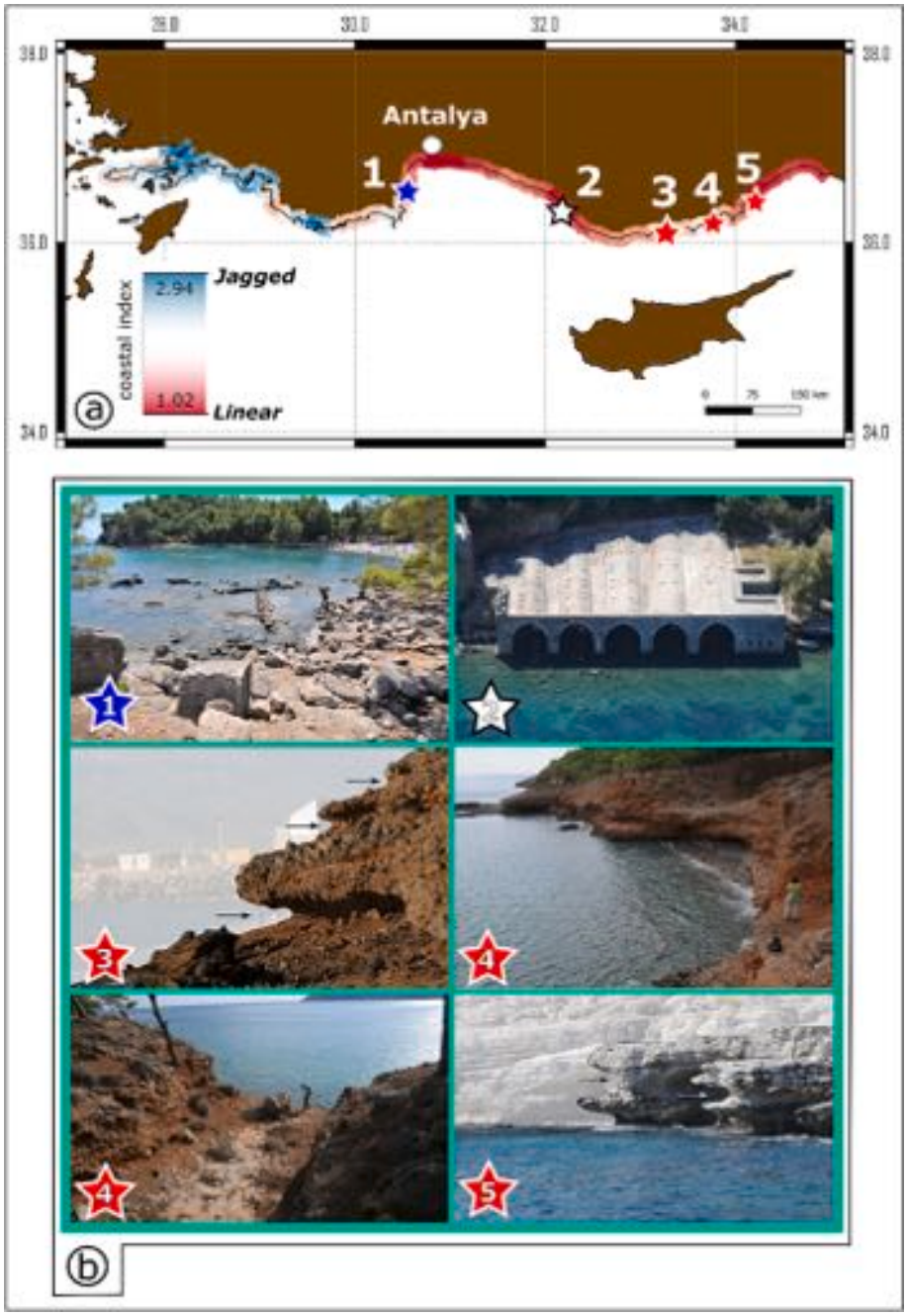

Fig. 15. a) A coastal index is calculated to highlight the variable coastal morphology. Stars represents the sites where other possible evidence for subsidence (blue star), uplift (red star) and stability (white star) could be found. b) 1 – Phaselis Harbour submerged structure; 2 – Shipyard in Alanya showing no appreciable variation around the sea-level since the time of construction (13th century CE); 3 – Uplifted notches Port of Yeşilovacık; 4) Uplifted notches and suspended valley near Mavikent; 5 – Uplifted notches in Narlikuyu. (For interpretation of the references to colour in this figure legend, the reader is referred to the web version of this article.)

coastal area of the CAP southern margin, we identify a vertical velocity jump in the range of 0.4 to 1.3 mm/yr between the CAP southern margin and the Hatay zone. This difference could be explained by the activity of the Ecemiş Fault Zone, which would imply that it accommodates the differential uplift of the southeastern margin of the Central Anatolian Plateau with respect to both the subsiding Adana-Cilicia Basin and the more slowly uplifting area of the Hatay Gulf.

For Syria and Lebanon, uplift rates range between 0.2 and 0.7 mm/yr, although Lebanon shows a more jagged profile, with late Holocene vertical velocities that reach up to 1.0 mm/yr. This higher variability could be related to the thrust faults of the Lebanese Restraining Bend (LRB), cutting and displacing the coastal area in several segments. Some of the paleo-coastline's elevation could include a co-seismic component, showing a vertical velocity that is not equilibrated to the long-term uplift rate. Such an equilibration of a crustal block affected by both co-seismic and long-term uplift rates can take a few thousand years (Elias et al., 2007).

The last clear vertical velocity jump occurs between Lebanon and Israel. Fish tanks and other pools in Israel (for a total of four), which indicate the sea level, are still in their original position, suggesting stability. It is worth noting how the RSL curves show an extremely accurate fitting of these markers. In fact, most of the RSL curves fall within the error bars of the pools; only the curves from Lambeck are at most 10 cm above. This information additionally confirms the the general coherence of the of GIA model predictions.

Although fish tanks show late Holocene stability (≈0 mm/yr) along the Israeli coast, other markers display different and less clear patterns. Most of the sea-level markers for Israel come from coastal wells and trottoirs of *Dendropoma petraeum*. These two different marker groups show quite different relationships with sea-level curves. Most of the wells are above the RSL curves, while *Dendropoma* samples are mostly under or overlap with the curves. The majority of the coastal wells come

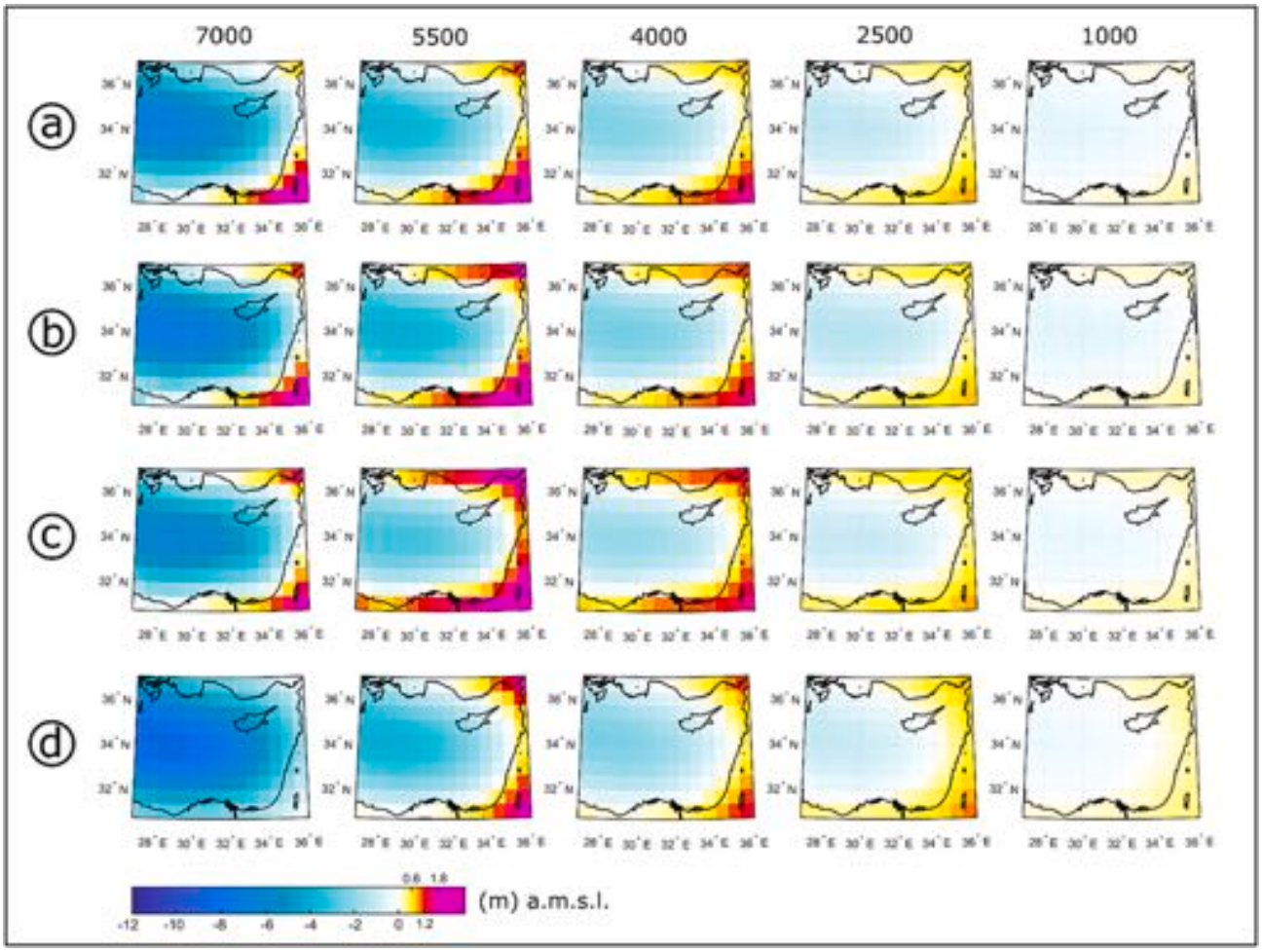

Fig. 16. – Prediction of sea-level at different times (7000, 5500, 4000, 2500, 1000 yr BP) for the different GIA models used in this paper: a) ICE-7G_NA(VM7) model solution from Peltier, b) ICE-6G(VM5a) model solution from Peltier, c) ICE-6G(VM5a) model solution from SELEN, d) ANU model solution from SELEN.

from the archaeological site of Caesarea, for which a fish tank instead indicates stability for the last 2000 yr (Anzidei et al., 2011). Considering the abundance of coastal wells that would be placed above sea level, Caesarea would be the only site from the Israeli coast showing a positive vertical velocity of 0.2 to 0.3 mm/yr, different from all the other sites where the velocity is between 0 and − 0.5 mm/yr. It has to be taken into consideration that RSL from coastal wells is based on archaeological assumptions and modern model and therefore has various uncertainties. Markers comprising *Dendropoma petraeum* trottoirs usually plot under the RSL curves with other kinds of markers such as terrestrial archaeological limiting points and a few wells coming from sites other than Caesarea. In this context, the Caesarea coastal wells seem to provide anomalous vertical velocities that contrast with other sea-level markers from the same site or neighboring areas. Indeed, from Caesarea and other adjacent sites, sea-level markers other than coastal wells show zero or slightly negative vertical velocities, in the range of 0 to −0.4 mm/yr. After excluding the coastal wells from Caesarea, all the sites show stability for the Israeli coast, or a low subsidence rate of about −0.4 mm/yr.

Late Holocene vertical velocity variability along the coast could be due to variation in the two components affecting the vertical velocity: a tectonic component, or a local scale component. For the case of Israel, the local component is probably related to compaction of sediments beneath some markers. This issue may particularly affect the oldest sites of the database, from ES61 to ES64. These sites comprise sea-level markers reported by Sivan et al. (2001), based on ^{14}C dating of terrestrial material. As shown from their RSL curves (Supplementary Material), these samples plot above the Lambeck solution and under the ICE-xG curves. Thus, vertical velocities calculated by using the Lambeck solution are highly positive in comparison with those calculated based on other RSL curves, which provide vertical velocities remarkably similar to those calculated considering younger markers. Therefore, for the coastal area of Israel, the ICE models seem to better fit older sea-level markers.

Given that the late Holocene vertical velocity for the coastal area of Israel is between 0 and − 0.5 mm/yr, the last velocity jump is identifiable between Lebanon and Israel. This change occurs near the political and geographic border between these two countries. Such a velocity change is also reported in Sivan et al. (2010), from a previous analysis based on data from vermetid trottoirs. As in other places showing a vertical velocity jump, some tectonic discontinuities are necessary to accommodate the differential late Holocene vertical velocities fields. Active thrusting may be related to the Lebanese Restraining Bend, as reported by Carton et al. (2009) and Elias et al. (2007) through seismic and bathymetric imaging. In addition, to the south, evidence for active normal faulting along vertical discontinuities, is also reported on the NE slope of the Carmel Mount (Carton et al., 2009).

5.2. *Insights from beachrocks of southern Turkey for reconstructions of vertical velocity field*

In the light of the late Holocene vertical velocity fields analysed in this work, from western Turkey to the Hatay Gulf, it is worth noting and discussing the different reconstructions reported in Desruelles et al.

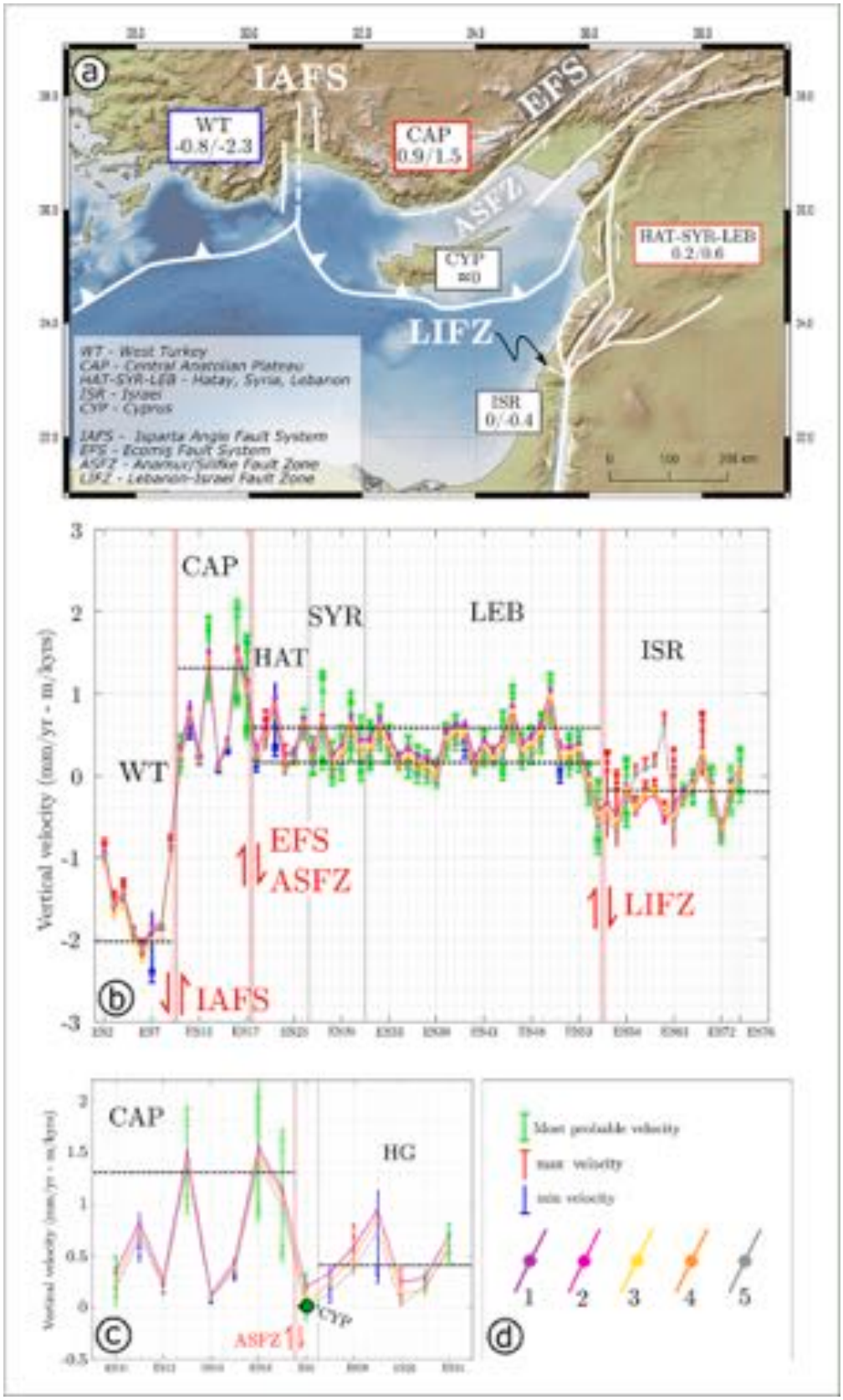

Fig. 17. Late Holocene vertical velocities along the Eastern Mediterranean coast: a) map view, b) projection along the coast without Cyprus, c) comparison between Cyprus and the adjacent continental sectors, Central Anatolian Plateau and Hatay coast.

a) Vertical velocity fields are reported inside the squares in mm/yr (equivalent to m/kyr). Red square contour means uplift, blue subsidence, and black stability.

b) Vertical velocity fields along a coastal profile from west Turkey to Israel passing through the CAP southern margin, the Hatay Gulf, Syria and Lebanon. Black vertical lines indicate borders of the different vertical velocity fields. Red vertical stripes are the main fault systems coinciding with the major vertical velocity jumps (>0.5 mm/yr). Each point is a site and therefore its vertical velocity is the mean velocity value from one or more relative sea-level markers related to that position. c) Comparison between the CAP southern margin, Cyprus, and the Hatay Gulf. Green bigger point is the manually corrected value for Cyprus (it is 0 mm/yr). d) Legend for the error bars and lines. Error bars are green if the velocity is found using only markers related to the paleo-MSL. Red error bars are for velocity obtained from terrestrial limiting points (sea-level markers that were for a certain amount higher than the MSL) and therefore are giving a maximum velocity estimate. Blue error bars are for velocity obtained from marine limiting points (sea-level markers that were for a certain amount under the MSL) and therefore are giving a minimum velocity estimate. Different colors of the lines stand for different velocity estimates depending on the model: 1-ICE-7G_NA(VM7) from Peltier's solution, 2-ICE-6G(VM5a) from Peltier's solution, 3- ICE-6G(VM5a) from SELEN low resolution settings, 4- ICE-6G (VM5a) from SELEN high resolution settings, 5-ANU-LW6(E-6) from SELEN solution.

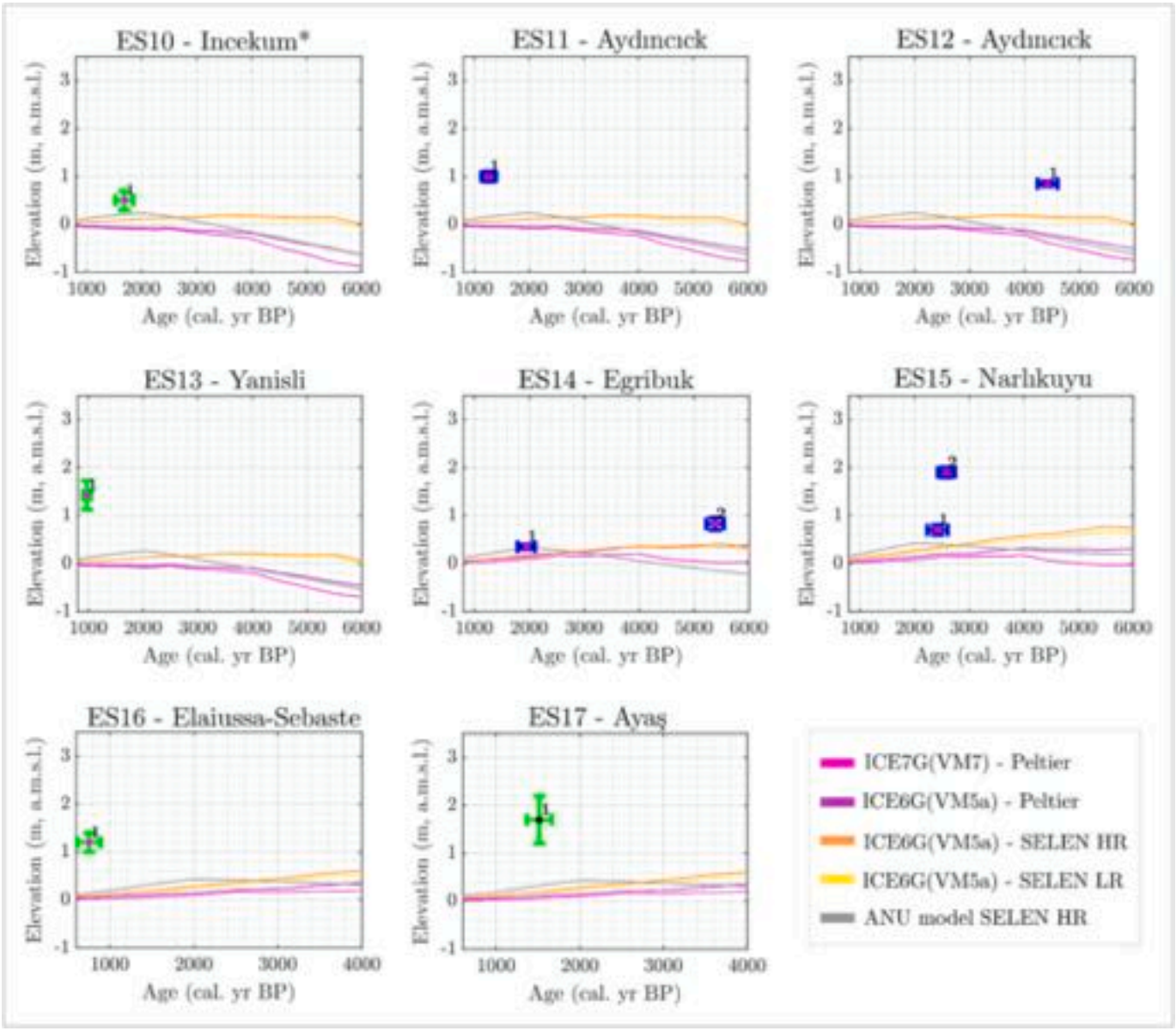

Fig. 18. RSL curves for the RSL markers along the coast of the CAP southern margin; ES10-Incekum* is the only site with data from published literature, it includes the RSL marker mentioned in Dalongeville and Sanlaville (1977) and Kelletat and Kayan (1983); ES11-ES17 are the new dated RSL markers. Green errorbars are for markers originally representing the paleo sea level whereas blue errorbars are RSL markers originally created at some depth under the sea level. Location and other information are in the Supplementary Material.

(2009). They report several beachrocks along the coast from Western Turkey to Hatay Gulf and provide the ages of two beachrocks, one to the west of Antalya and one on the Hatay coast. All the data from beachrocks are summarized in Fig. 12 and Tables 1 and 2.

Although the results from Desruelles et al. (2009) show some similarities to the vertical velocity fields reconstructed here, there are some important differences. First, based on the dated beachrocks in the Hatay Gulf, Desruelles et al. (2009) report subsidence at a rate of −0.13 to −0.14 mm/yr, whereas our results based on notches show uplift of 0.2 to 0.8 mm/yr. Drowned beachrocks in Hatay (Fig. 12) appear to contradict the well-documented raised Holocene coastlines from the same area (Pirazzoli et al., 1991; Sanlaville et al., 1997). The inconsistency between these different datasets could be due to the different locations of the beachrocks and the notches, which are potentially separated by some faults. Apart from this possibility, younger carbon contamination in the diagenetic carbonate cement of the beachrocks cannot be excluded. For a reliable ^{14}C date on beachrock, the cementation should have occurred during detrital grain deposition, through a unique phase of cement precipitation. However, after diagenesis, multiple cementing events with younger-C fluid contamination cannot be ruled out (Pisapia et al., 2018).

Additional differences are apparent when comparing the beachrocks with other kinds of sea-level markers along the coastal area of the CAP southern margin. Overall, late Holocene vertical velocities from beachrocks are consistently lower than the velocities evaluated from other sea-level markers. In Fig. 17, most of the RSL curves fall within the vertical uncertainty of the elevation of the beachrocks BCR9 and BCR10.1. Assuming the lowest vertical velocity value of 1.0 mm/yr, evaluated through other sea-level markers, both the beachrocks should be well above the highest prediction of the models. These differences could be explained by assuming a vertical component of the velocity field that counteracts the tectonic component. In this case, the additional vertical component would lower the elevation of the beachrocks. Post-depositional compaction of the beachrock and its substratum could

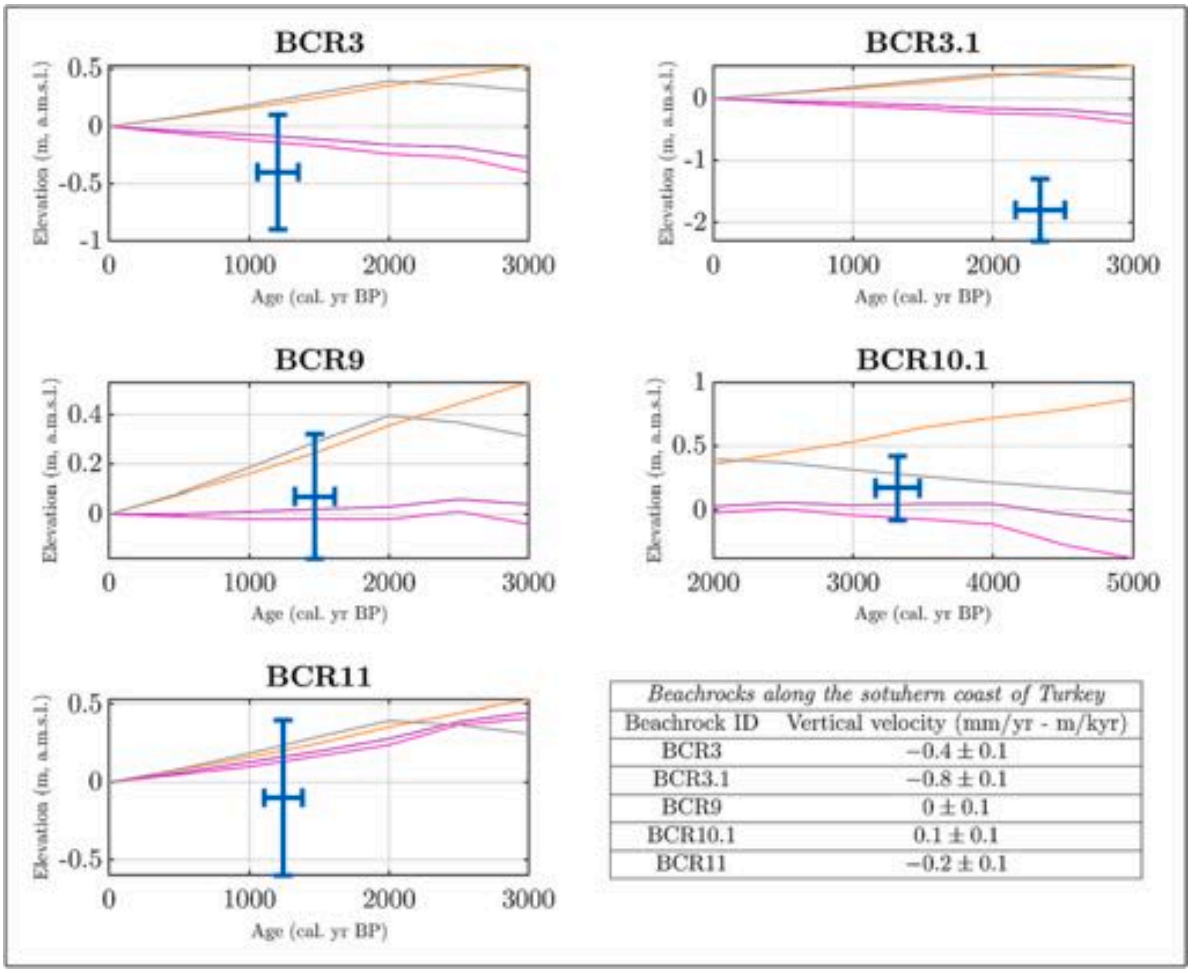

Beachrocks along the sotuhern coast of Turkey	
Beachrock ID	Vertical velocity (mm/yr - m/kyr)
BCR3	-0.4 ± 0.1
BCR3.1	-0.8 ± 0.1
BCR9	0 ± 0.1
BCR10.1	0.1 ± 0.1
BCR11	-0.2 ± 0.1

Fig. 19. RSL curves for the dated beachrocks along the southern coast of Turkey. RSL curves have the same colors as in Fig. 17 and Fig. 18.

induce this lowering. Assuming that the beachrocks developed on soft coastal sediments, compaction dynamics of the underlying sediment, responsible for a local subsidence, could be taken into account. Alternatively, a local downward component due to normal faulting cannot be excluded.

6. Conclusions

Our review and reassessment of the late Holocene relative sea-level markers along the easternmost Mediterranean coast, from western Turkey to Israel, integrates new and previously published data to revise the late Holocene vertical velocity field. The dataset used in this work includes data from literature, as well as new sea-level markers from the coastal area of the CAP southern margin (southern Turkey). The new data fill a gap of Holocene RSL information along the Eastern Mediterranean coast between western Turkey and Israel. All the elevations of the sea-level markers used in this work have been corrected the most updated and tested GIA models, to better define the vertical velocity fields of the investigated areas. The results of this review call attention to several crucial points regarding the late Holocene differential uplift that characterize the Eastern Mediterranean coastal area. The main points of conclusion are summarized as follows:

1. New data from late Holocene sea-level markers along the coast of the CAP southern margin document active uplift, which is the tail of the rapid uplift event that affected the area in the middle Pleistocene (Öğretmen et al., 2018), with a peak of uplift at ca. 200 ka (3.8 m/kyr, Racano et al., 2020, 2021). Positive late Holocene vertical velocity estimates for the CAP southern margin range from 0.9 to 1.5 mm/yr, corroborating uplift predictions from modeling marine terrace sequences (1.2 to 1.6 mm/yr; Racano et al., 2020).
2. The vertical velocity distribution along the Eastern Mediterranean coastal areas defines vertical velocity fields bounded by the major active fault zones affecting the study area, which distinguish kinematically separated crustal blocks characterized by differential late Holocene vertical movements.
3. The crustal block to the west of Antalya shows negative vertical velocities ranging from −0.8 to −2.3 mm/yr, which are similar to those reported in Anzidei et al. (2011). The Isparta Angle Fault Zone seems to be the boundary between this negative vertical velocity field, which pertains to the Western Anatolia Extensional Province (Şengör et al., 1985), and the uplifting coastal area of the CAP southern margin.
4. The crustal block containing the CAP southern margin shows a vertical velocity field typified by positive values between 0.9 and 1.5 mm/yr, even though the western margin of this crustal block, between the Isparta Angle Fault System and the Kirkkavak Fault, seems to show lower values of uplift (≈0.3 mm/yr). The kinematic boundary between this uplifting crustal block and the more slowly uplifting or stationary surrounding regions occurs along the southwestern extension of the Ecemiş Fault Zone and the Anamur-Silifke Fault Zone.
5. The crustal block to the south of these fault zones, which comprises Cyprus and the Hatay Gulf, shows vertical stability for Cyprus, whereas the Hatay Gulf shows positive late Holocene vertical velocities of 0.2 to 0.6 mm/yr, depending on the adopted GIA model.

6. Late Holocene vertical velocities from beachrocks seem to be lower than the velocities derived from other markers. Those differences can be explained by assuming a local component of the vertical velocity field that counteracts the regional tectonic uplift affecting the area. This local component could be due to the post-depositional compaction dynamics of the beachrocks, as well as a local downward component can be related to normal faulting. Alternatively, younger carbon contamination in the dated diagenetic carbonate cement of the beachrocks cannot be excluded.
7. The Levant coastal area, except for Israel, shows positive vertical velocities in the range of 0.1 to 0.6 mm/yr. This positive vertical velocity field is mainly related to the Lebanese Restraining Bend, which also affects the Lebanese coastal area. Peak uplift rates of >1 mm/yr are interpreted to be related to a co-seismic component of uplift, altering the uplift rate averaged over thousands of years.
8. In the Israeli coastal area, some ambiguities and inconsistences in the vertical velocity measurements are likely due to the wide variety of sea-level markers used. According to the fish tanks along the Israeli coast, no vertical movements occurred within the last 2.0 to 2.5 kyr. In contrast, analyses of *Dendropoma petraum* trottoirs yield low negative vertical velocities (slight subsidence, between −0.1 and −0.4 mm/yr). In Israel, coastal wells are sea-level markers coming almost exclusively from a single site in Caesarea. All these wells point to positive low velocities (0.3 mm/yr), in contrast with all the other evidence along the same coast. Given these inconsistences, we question the reliability of the sea-level meaning of some of these markers, but additional analysis is needed to understand whether a methodological bias or a geological process could explain these differences. Nevertheless, in Israel, late Holocene vertical velocities are clearly lower than the vertical velocities affecting the adjacent coastal area of Lebanon. The difference between these two vertical velocity fields can be explained by vertical slip along some active faults separating the Israeli and Lebanon coastal sectors.
9. Fish tanks, found along the coast at the same level of their original position, represent a valuable opportunity to test the GIA models used in this analysis. RSL curves for Israel, especially the ICE types, show a perfect match with the sea-level markers dated between 2000 and 2500 yr BP. This observation supports the reliability of GIA predictions used for other markers in this time interval. In contrast, ICE curves show a slightly worse fit for a fish tank in Cyprus. In this case, all the ICE solutions lie 30–40 cm below the lower uncertainty of the sea-level marker. In contrast, the ANU solution from SELEN shows a better match. Given these results and according to all the tests performed in the coastal area of the Western Mediterranean, it is not possible to find a best model: ICE-type seem to better fit data along the coast of the continent, whereas the ANU model seems to better fit the only stable marker in Cyprus. All the solutions used in this work could be considered as the most accurate estimates of past late Holocene relative sea-level predictions in the Mediterranean region.

Data availability

The database of the Eastern Mediterranean Holocene sea-level markers, together with the detailed results of the vertical velocity analysis described in the text, are available at the link: https://data.mendeley.com/v1/datasets/vp3cr74n7g/draft?preview=1.

Declaration of Competing Interest

The authors declare that they have no known competing financial interests or personal relationships that could have appeared to influence the work reported in this paper.

Acknowledgments

This study is part of the Anatolian Plateau Climate and Tectonic Hazards (ALErT) project, funded by the European Union Marie Curie Actions “Innovative Training Networks” program (FP7-PEOPLE-2013-ITN) (grant agreement 607996). The grant to the Department of Science of Roma Tre University (MIUR—Italy Department of Excellence, article 1, paragraph 314–337, law 232/2016) and the PRIN2017 Project 20177BX42Z_001 funded by MIUR-Italy are gratefully acknowledged. We would like to thank Daniele Melini of the National Institute of Geophysics and Volcanology, for calculating the sea level curves and for supporting in the analysis. We would then like to thank W. R. Peltier and his research team for providing the sea level curves with his models. Thanks also to Taylor Schildgen for valuable scientific advice and English language review.

References

Aksu, A.E., Calon, T., Hall, J., Kurtboğan, B., Gürçay, S., Çifçi, G., 2014. Complex interactions fault fans developed in a strike-slip system: Kozan Fault ZoneEastern Mediterranean Sea. Marine Geol. 351, 91–107.

Aksu, A.E., Hall, J., Yaltırak, C., 2021. The uppermost Messinian-Quaternary evolution of the Anamur-Kormakiti Zone: the transition between the Outer Cilicia and Antalya basins, northeastern Mediterranean. Marine Petrol. Geol. https://doi.org/10.1016/j.marpetgeo.2021.105451.

Antonioli, F., Ferranti, L., Lambeck, K., Kershaw, S., Verrubbi, V., Dai Pra, G., 2006. Late Pleistocene to Holocene record of changing uplift rates in southern Calabria and northeastern Sicily (southern Italy, Central Mediterranean Sea). Tectonophysics 422 (1–4), 23–40.

Antonioli, F., Presti, V.L., Rovere, A., Ferranti, L., Anzidei, M., Furlani, S., Spampinato, C. R., 2015. Tidal notches in Mediterranean Sea: a comprehensive analysis. Quat. Sci. Rev. 119, 66–84.

Anzidei, M., Antonioli, F., Benini, A., Lambeck, K., Sivan, D., Serpelloni, E., Stocchi, P., 2011. Sea level change and vertical land movements since the last two millennia along the coasts of southwestern Turkey and Israel. Quat. Int. 232 (1–2), 13–20.

Argus, D.F., Peltier, W.R., Drummond, R., Moore, A.W., 2014. The Antarctica component of postglacial rebound model ICE-6G_C (VM5a) based on GPS positioning, exposure age dating of ice thicknesses, and relative sea level histories. Geophys. J. Int. 198 (1), 537–563.

Auriemma, R., Solinas, E., 2009. Archaeological remains as sea level change markers: a review. Quat. Int. 206 (1–2), 134–146.

Ballato, P., Uba, C.E., Landgraf, A., Strecker, M.R., Sudo, M., Stockli, D.F., Tabatabaei, S. H., 2011. Arabia-Eurasia continental collision: Insights from late Tertiary foreland-basin evolution in the Alborz Mountains, northern Iran. Bulletin 123 (1–2), 106–131.

Barazangi, M., Sandvol, E., Seber, D., 2006. Structure and tectonic evolution of the Anatolian plateau in eastern Turkey. Geol. Soc. Am.

Beltrame, C., 2012. Archeologia marittima del Mediterraneo: navi, merci e porti dall'antichità all'età moderna. Carocci Ed.

Bennett, R.A., Hreinsdóttir, S., 2007. Constraints on vertical crustal motion for long baselines in the central Mediterranean region using continuous GPS. Earth Planet. Sci. Lett. 257 (3–4), 419–434.

Biryol, C.B., Beck, S.L., Zandt, G., Özacar, A.A., 2011. Segmented african lithosphere beneath the Anatolian region inferred from teleseismic P-wave tomography. Geophys. J. Int. 184, 1037–1057. https://doi.org/10.1111/j.1365-246X.2010.04910.x.

Boaretto, E., Mienis, H.K., Sivan, D., 2010. Reservoir age based on pre-bomb shells from the intertidal zone along the coast of Israel. Nucl. Inst. Methods Phys. Res. Sect. B: Beam Interact. Mater. Atoms 268 (7–8), 966–v.

Bonino, M., 2018. A further proposal for the hull lines of the Madrague de Giens Ship (c. 70 BC). Int. J. Naut. Archaeol. 47 (2), 443–459.

Blackmail, D.J., 1973. The harbours of Phaselis. Int. J. Naut. Archaeol. 2 (2), 355–364.

Carton, H., Singh, S.C., Tapponnier, P., Elias, A., Briais, A., Sursock, A., Barrier, L., 2009. Seismic evidence for Neogene and active shortening offshore of Lebanon (Shalimar cruise). J. Geophys. Res. Solid Earth 114 (B7).

Ciner, A., Desruelles, S., Fouache, E., Kosun, E., Dalongeville, R., 2009. Beachrock formations on the Mediterranean Coast of Turkey: Implications for Holocene Sea level changes and tectonics. Turk. Jeol. Bulteni-Geol. Bull. Turk. 52 (3), 257–296.

Cosentino, D., Schildgen, T.F., Cipollari, P., Faranda, C., Gliozzi, E., Hudáčková, N., Strecker, M.R., 2012. Late Miocene surface uplift of the southern margin of the Central Anatolian Plateau, Central TauridesTurkey. Geol. Soc. Am. Bull. 124 (1–2), 133–145.

Dağgülü, İ.B., 2009. A 13th-Century Shipyard at Alanya (Alaiyye), on the Mediterranean Coast of Turkey. Int. J. Naut. Archaeol. 38 (1), 13–20.

Dalongeville, R., Sanlaville, P., 1977. Témoins de lignes de rivage holocènes en Turquie méridionale. Quaternaire 14 (4), 79–81.

Dalongeville, R., Laborel, J., Pirazzoli, P.A., Sanlaville, P., Arnold, M., Bernier, P., Montaggioni, L., 1993. Les variations récentes de la ligne de rivage Sur le littoral syrien. Quaternaire 4 (1), 45–53.

Dean, S., Horton, B.P., Evelpidou, N., Cahill, N., Spada, G., Sivan, D., 2019. Can we detect centennial sea-level variations over the last three thousand years in israeli archaeological records? Quat. Sci. Rev. 210, 125–135.

Desruelles, S., Fouache, É., Ciner, A., Dalongeville, R., Pavlopoulos, K., Kosun, E., Potdevin, J.L., 2009. Beachrocks and sea level changes since Middle Holocene: comparison between the insular group of Mykonos–Delos–Rhenia (Cyclades, Greece) and the southern coast of Turkey. Glob. Planet. Chang. 66 (1–2), 19–33.
Dickinson, W.R., 2000. Hydro-isostatic and tectonic influences on emergent Holocene paleoshorelines in the Mariana Islands, western Pacific Ocean. J. Coast. Res. 735–746.
Elias, A., Tapponnier, P., Singh, S.C., King, G.C., Briais, A., Daëron, M., Klinger, Y., 2007. Active thrusting offshore Mount Lebanon: source of the tsunamigenic AD 551 Beirut-Tripoli earthquake. Geology 35 (8), 755–758.
Evelpidou, N., Karkani, A., 2018. Archaeology and sea-level change. Encyclopedia of Coastal Science. In: Makowski, C. (Ed.), In: Encyclopedia of Earth Sciences Series. Springer, pp. 67–73.
Ferrazzoli, A.F., Ricci, M., 2009. In: Cilician Ceramic Production from Roman to byzantine AgeNew Data From Elaiussa Sebaste, 17, pp. 23–44. Olba.
Flemming, N.C., 1969. Introduction. Archaeological evidence for eustatic change of sea level and earth movements in the Western Mediterranean during the last 2000 years, Vol. 109. Geological Society of America, pp. 3–12.
Galili, E., Şevketoğlu, M., Salamon, A., Zviely, D., Mienis, H.K., Rosen, B., Moshkovitz, S., 2016. Late Quaternary beach deposits and archaeological relicts on the coasts of Cyprus, and the possible implications of sea-level changes and tectonics on the early populations. Geol. Soc. Lond., Spec. Publ. 411 (1), 179–218.
Gibson, R., Atkinson, R., Gordon, J., 2006. Mediterranean coralligenous assemblages: a synthesis of present knowledge. Oceanogr. Mar. Biol. Annu. Rev. 44, 123–195.
Giménez, J., Suriñach, E., Fleta, J., Goula, X., 1996. Recent vertical movements from high-precision leveling data in Northeast Spain. Tectonophysics 263 (1–4), 149–161.
Glover, C., Robertson, A., 1998. Neotectonic intersection of the Aegean and Cyprus tectonic arcs: extensional and strike-slip faulting in the Isparta AngleSW Turkey. Tectonophysics 298 (1–3), 103–132.
Göğüş, O.H., Pysklywec, R.N., 2008. Mantle lithosphere delamination driving plateau uplift and synconvergent extension in eastern Anatolia. Geology 36 (9), 723–726.
Gregory, J.M., Griffies, S.M., Hughes, C.W., Lowe, J.A., Church, J.A., Fukimori, I., Ponte, R.M., 2019. Concepts and terminology for sea level: mean, variability and change, both local and global. Surv. Geophys. 40 (6), 1251–1289.
Hall, J., Aksu, A.E., King, H., Gogacz, A., Yaltırak, C., Çifçi, G., 2014. Miocene–Recent evolution of the western Antalya Basin and its linkage with the Isparta Angle, eastern Mediterranean. Marine Geol. 349, 1–23.
Heaton, T.J., Köhler, P., Butzin, M., Bard, E., Reimer, R.W., Austin, W.E., Skinner, L.C., 2020. Marine20—the marine radiocarbon age calibration curve (0–55,000 cal BP). Radiocarbon 62 (4), 779–820.
Hershkovitz, I., Weber, G.W., Quam, R., Duval, M., Grün, R., Kinsley, L., Arsuaga, J.L., 2018. The earliest modern humans outside Africa. Science 359 (6374), 456–459.
Hijma, M.P., Engelhart, S.E., Törnqvist, T.E., Horton, B.P., Hu, P., Hill, D.F., 2015. A protocol for a geological sea-level database. In: Shennan, I., Long, A.J., Horton, B. P. (Eds.), Handbook of Sea-Level Research. Wiley Blackwell, pp. 536–553.
Howell, A., Jackson, J., Copley, A., McKenzie, D., Nissen, E., 2017. Subduction and vertical coastal motions in the eastern Mediterranean. Geophys. J. Int. 211 (1), 593–620.
Jackson, J., McKenzie, D., 1984. Active tectonics of the Alpine—Himalayan Belt between western Turkey and Pakistan. Geophys. J. Int. 77 (1), 185–264.
Jaffey, N., Robertson, A.H.F., 2001. New sedimentological and structural data from the Ecemis Fault Zone, southern Turkey: implications for its timing and offset and Cenozoic tectonic escape of Anatolia. J. Geol. Soc. Lond. 158, 367–378.
Khan, N.S., Ashe, E., Shaw, T.A., Vacchi, M., Walker, J., Peltier, W.R., Horton, B.P., 2015. Holocene relative sea-level changes from near-, intermediate-, and far-field locations. Curr. Clim. Change Rep. 1 (4), 247–262.
Johansson, J.M., Davis, J.L., Scherneck, H.G., Milne, G.A., Vermeer, M., Mitrovica, I.X., Shapiro, I.I., 2002. Continuous GPS measurements of postglacial adjustment in Fennoscandia 1. Geodetic results. J. Geophys. Res. Solid Earth 107 (B8), ETG–3.
Kelletat, D., Kayan, I., 1983. Alanya batisindaki kiyilarda ilk C 14 tarihlendirmelerinin Isiginda Geç Holosen tektonik hareketleri. (First 14 C datings and Late Holocene tectonic events on the Mediterranean coastline, west of Alanya, southern Turkey). Türk. Jeol. Kurumu Bülteni Ankara 26, 83–87.
Kopp, R.E., Hay, C.C., Little, C.M., Mitrovica, J.X., 2015. Geographic variability of sea-level change. Curr. Clim. Change Rep. 1 (3), 192–204.
Laborel, J., Laborel-Deguen, F., 1996. Biological indicators of Holocene sea-level and climatic variations on rocky coasts of tropical and subtropical regions. Quat. Int. 31, 53–60.
Laborel, J., Laborel-Deguen, F., 2005. Sea-level indicators, biologic. Encycl. Coast. Sci. 833–834.
Lambeck, K., Purcell, A., 2005. Sea-level change in the Mediterranean Sea since the LGM: model predictions for tectonically stable areas. Quat. Sci. Rev. 24 (18–19), 1969–1988.
Lambeck, K., Rouby, H., Purcell, A., Sun, Y., Sambridge, M., 2014. Sea level and global ice volumes from the Last Glacial Maximum to the Holocene. Proc. Natl. Acad. Sci. 111 (43), 15296–15303.
Lambeck, K., Purcell, A., Zhao, S., 2017. The North American Late Wisconsin ice sheet and mantle viscosity from glacial rebound analyses. Quat. Sci. Rev. 158, 172–210.
Le Pichon, X., Angelier, J., 1979. The Hellenic arc and trench system: a key to the neotectonic evolution of the eastern Mediterranean area. Tectonophysics 60 (1–2), 1–42.
Martinec, Z., Klemann, V., van der Wal, W., Riva, R.E.M., Spada, G., Sun, Y., James, T.S., 2018. A benchmark study of numerical implementations of the sea level equation in GIA modelling. Geophys. J. Int. 215 (1), 389–414.
Mauz, B., Vacchi, M., Green, A., Hoffmann, G., Cooper, A., 2015a. Beachrock: a tool for reconstructing relative sea level in the far-field. Mar. Geol. 362, 1–16.
Mauz, B., Ruggieri, G., Spada, G., 2015b. Terminal Antarctic melting inferred from a far-field coastal site. Quat. Sci. Rev. 116, 122–132.
McClusky, S., Balassanian, S., Barka, A., Demir, C., Ergintav, S., Georgiev, I., Veis, G., 2000. Global Positioning System constraints on plate kinematics and dynamics in the eastern Mediterranean and Caucasus. J. Geophys. Res. Solid Earth 105 (B3), 5695–5719.
McKenzie, D.P., 1970. Plate tectonics of the Mediterranean region. Nature 226 (5242), 239–243.
McKenzie, D., 1978. Active tectonics of the Alpine—Himalayan belt: the Aegean Sea and surrounding regions. Geophys. J. Int. 55 (1), 217–254.
Milne, G.A., Gehrels, W.R., Hughes, C.W., Tamisiea, M.E., 2009. Identifying the causes of sea-level change. Nat. Geosci. 2 (7), 471–478.
Melis, R., Bernasconi, M.P., Colizza, E., Di Rita, F., Schneider, E.E., Forte, E., Ricci, M., 2015. Late Holocene palaeoenvironmental evolution of the northern harbour at the Elaiussa Sebaste archaeological site (south-eastern Turkey): evidence from core ELA6. Turk. J. Earth Sci. 24 (6), 566–584.
Mitrovica, J.X., Milne, G.A., 2002. On the origin of late Holocene sea-level highstands within equatorial ocean basins. Quat. Sci. Rev. 21 (20–22), 2179–2190.
Morhange, C., Pirazzoli, P.A., Marriner, N., Montaggioni, L.F., Nammour, T., 2006. Late Holocene relative sea-level changes in Lebanon,Eastern Mediterranean. Marine Geol. 230 (1–2), 99–114.
Morhange, C., Marriner, N., 2015. Archeological and biological relative sea-level indicators. In: Handbook of Sea-level Research, pp. 146–156.
Öğretmen, N., Cosentino, D., Gliozzi, E., Cipollari, P., Yıldırım, C., 2015. Holocene extensional faulting at the southeastern margin of the Central Anatolian Plateau: implications for the kinematics of the Ecemiş Fault Zone (Mersin, southern Turkey). In: 6th International INQUA Meeting on Paleoseismology, Active Tectonics and Archaeoseismology, 19-24 April 2015, Pescina, Fucino Basin, Italy, 27. Miscellanea INGV, pp. 325–328.
Mourtzas, N., Kolaiti, E., Anzidei, M., 2016. Vertical land movements and sea level changes along the coast of Crete (Greece) since Late Holocene. Quater. Int. 401, 43–70.
Öğretmen, N., Cipollari, P., Frezza, V., Faranda, C., Karanika, K., Gliozzi, E., Cosentino, D., 2018. Evidence for 1.5 km of uplift of the Central Anatolian Plateau's southern margin in the last 450 kyr and implications for its multiphased uplift history. Tectonics 37 (1), 359–390.
Över, S., Özden, S., Kamacı, Z., Yılmaz, H., Ünlügenç, U.C., Pınar, A., 2016. Upper crust response to geodynamic processes beneath Isparta Angle, SW Turkey: revealed by CMT solutions of earthquakes. Tectonophysics 687, 94–104.
Ozel, E., Ulug, A., Pekcetinoz, B., 2007. Neotectonic aspects of the northern margin of the Adana-Cilicia submarine basin, NE Mediterranean. J. Earth Syst.Sci. 116 (2), 113–124.
Pappalardo, M., 2019. Storia della vela: Tra commercio, guerra e sport. HOEPLI EDITORE.
Peltier, W.R., 2004. Global glacial isostasy and the surface of the ice-age Earth: the ICE-5G (VM2) model and GRACE. Annu. Rev. Earth Planet. Sci. 32, 111–149.
Peltier, W.R., Argus, D.F., Drummond, R., 2015. Space geodesy constrains ice age terminal deglaciation: The global ICE-6G_C (VM5a) model. J. Geophys. Res. Solid Earth 120 (1), 450–487.
Pirazzoli, P.A., Laborel, J., Saliège, J.F., Erol, O., Kayan, I., Person, A., 1991. Holocene raised shorelines on the Hatay coasts (Turkey): palaeoecological and tectonic implications. Mar. Geol. 96 (3–4), 295–311.
Pirazzoli, P.A., Stiros, S.C., Arnold, M., Laborel, J., Laborel-Deguen, F., Papageorgiou, S., 1994. Episodic uplift deduced from Holocene shorelines in the Perachora Peninsula, Corinth area,Greece. Tectonophysics 229 (3–4), 201–209.
Peltier, W.R., Fairbanks, R.G., 2006. Global glacial ice volume and Last Glacial Maximum duration from an extended Barbados sea level record. Quater. Sci. Rev. 25 (23–24), 3322–3337.
Pirazzoli, P.A., Evelpidou, N., 2013. Tidal notches: a sea-level indicator of uncertain archival trustworthiness. Palaeogeogr. Palaeoclimatol. Palaeoecol. 369, 377–384.
Pisapia, C., Deschamps, P., Battani, A., Buschaert, S., Guihou, A., Hamelin, B., Brulhet, J., 2018. U/Pb dating of geodic calcite: new insights on Western Europe major tectonic events and associated diagenetic fluids. J. Geol. Soc. 175 (1), 60–70.
Price, S., Higham, T., Nixon, L., Moody, J., 2002. Relative sea-level changes in Crete: reassessment of radiocarbon dates from Sphakia and west Crete. In: The Annual of the British School at Athens, pp. 171–200.
Racano, S., Jara-Muñoz, J., Cosentino, D., Melnick, D., 2020. Variable Quaternary uplift along the southern margin of the Central Anatolian Plateau inferred from modeling marine terrace sequences. Tectonics 39, e2019TC005921. https://doi.org/10.1029/2019TC005921.
Racano, S., Schildgen, T.F., Cosentino, D., Miller, S.R., 2021. Temporal and spatial variations in uplift from river-profile inversions at the Central Anatolian Plateau southern margin. J. Geophys. Res. Earth Surf. 126, e2020JF006027 https://doi.org/10.1029/2020JF006027.
Radeff, G., Schildgen, T.F., Cosentino, D., Strecker, M.R., Cipollari, P., Darbaş, G., Gürbüz, K., 2017. Sedimentary evidence for late Messinian uplift of the SE margin of the Central Anatolian Plateau: Adana Basin, southern Turkey. Basin Res. 29, 488–514.
Ramsey, C.B., 1995. Radiocarbon calibration and analysis of stratigraphy: the OxCal program. Radiocarbon 37 (2), 425–430.
Reilinger, R.E., McClusky, S.C., Oral, M.B., King, R.W., Toksoz, M.N., Barka, A.A., Sanli, I., 1997. Global Positioning System measurements of present-day crustal movements in the Arabia-Africa-Eurasia plate collision zone. J. Geophys. Res. Solid Earth 102 (B5), 9983–9999.
Reilinger, R., McClusky, S., Vernant, P., Lawrence, S., Ergintav, S., Cakmak, R., Karam, G., 2006. GPS constraints on continental deformation in the Africa-Arabia-

Eurasia continental collision zone and implications for the dynamics of plate interactions. J. Geophys. Res. Solid Earth 111 (B5).
Reimer, P.J., Austin, W.E., Bard, E., Bayliss, A., Blackwell, P.G., Ramsey, C.B., Talamo, S., 2020. The IntCal20 Northern Hemisphere radiocarbon age calibration curve (0–55 cal kBP). Radiocarbon 62 (4), 725–757.
Reimer, P.J., McCormac, F.G., 2002. Marine radiocarbon reservoir corrections for the Mediterranean and Aegean Seas. Radiocarbon 44 (1), 159–166.
Rovere, A., Antonioli, F., Bianchi, C.N., 2015. Fixed biological indicators. In: Handbook of Sea-Level Research, pp. 268–280.
Rovere, A., Stocchi, P., Vacchi, M., 2016. Eustatic and relative sea level changes. Curr. Clim. Change Rep. 2 (4), 221–231.
Roy, K., Peltier, W.R., 2018. Relative sea level in the Western Mediterranean basin: a regional test of the ICE-7G_NA (VM7) model and a constraint on late Holocene Antarctic deglaciation. Quat. Sci. Rev. 183, 76–87.
Sanlaville, P., Dalongeville, R., Bernier, P., Evin, J., 1997. The Syrian coast: a model of Holocene coastal evolution. J. Coast. Res. 385–396.
Schiaparelli, S., Albertelli, G., Cattaneo-Vietti, R., 2006. Phenotypic plasticity of Vermetidae suspension feeding: a potential bias in their use as Biological Sea-Level Indicators. Mar. Ecol. 27 (1), 44–53.
Schildgen, T.F., Cosentino, D., Bookhagen, B., Niedermann, S., Yıldırım, C., Echtler, H., Strecker, M.R., 2012a. Multi-phased uplift of the southern margin of the Central Anatolian plateau, Turkey: A record of tectonic and upper mantle processes. Earth Planet. Sci. Lett. 317, 85–95.
Schildgen, T.F., Cosentino, D., Caruso, A., Buchwaldt, R., Yildirim, C., Rojay, B., Strecker, M.R., 2012b. Surface expression of eastern Mediterranean slab dynamics: Neogene topographic and structural evolution of the southwest margin of the Central Anatolian Plateau, Turkey. Tectonics 31, TC2005. https://doi.org/10.1029/2011TC003021.
Schildgen, T.F., Yıldırım, C., Cosentino, D., Strecker, M.R., 2014. Linking slab break-off, Hellenic trench retreat, and uplift of the Central and Eastern Anatolian plateaus. Earth Sci. Rev. 128, 147–168. https://doi.org/10.1016/j.earscirev.2013.11.006.
Şengör, A.M.C., Özeren, S., Genç, T., Zor, E., 2003. East Anatolian high plateau as a mantle-supported, north-south shortened domal structure. Geophys. Res. Lett. 30 (24).
Şengör, A.M.C., Kidd, W.S.F., 1979. Post-collisional tectonics of the Turkish-Iranian Plateau and a comparison with Tibet. Tectonophysics 55, 361–376.
Şengör, A.M.C., Görür, N., Şaroğlu, F., 1985. Strike-slip faulting and related basin formation in zones of tectonic escape: Turkey as a case study. In: Biddle, K., Christie-Blick, N. (Eds.), Strike-slip Deformation, Basin Formation and Sedimentation, 37. Soc. of Econ. Paleont. and Miner., Spec. Publ, pp. 227–264.
Sivan, D., Wdowinski, S., Lambeck, K., Galili, E., Raban, A., 2001. Holocene sea-level changes along the Mediterranean coast of Israel, based on archaeological observations and numerical model. Palaeogeogr. Palaeoclimatol. Palaeoecol. 167 (1–2), 101–117.
Simons, M., Fialko, Y., Rivera, L., 2002. Coseismic deformation from the 1999 M w 7.1 Hector Mine, California, earthquake as inferred from InSAR and GPS observations. Bull. Seismol. Soc. Am. 92 (4), 1390–1402.
Sivan, D., Schattner, U., Morhange, C., Boaretto, E., 2010. What can a sessile mollusk tell about neotectonics? Earth Planet. Sci. Lett. 296 (3–4), 451–458.
Spada, G., Stocchi, P., 2007. SELEN: A Fortran 90 program for solving the "sea-level equation". Comput. Geosci. 33 (4), 538–562.
Spada, G., Melini, D., 2019. SELEN 4 (SELEN version 4.0): a Fortran program for solving the gravitationally and topographically self-consistent sea-level equation in glacial isostatic adjustment modeling. Geosci. Model Dev. 12 (12), 5055–5075.
Spampinato, C.R., Braitenberg, C., Monaco, C., Scicchitano, G., 2013. Analysis of vertical movements in eastern Sicily and southern Calabria (Italy) through geodetic leveling data. J. Geodyn. 66, 1–12.
Stuiver, M., Polach, H.A., 1977. Discussion reporting of 14 C data. Radiocarbon 19 (3), 355–363.
Stuiver, M., Reimer, P.J., 1993. Extended 14 C data base and revised CALIB 3.0 14 C age calibration program. Radiocarbon 35 (1), 215–230.
Stuiver, M., Reimer, P.J., Bard, E., Beck, J.W., Burr, G.S., Hughen, K.A., Spurk, M., 1998. INTCAL98 radiocarbon age calibration, 24,000–0 cal BP. radiocarbon, 40(3), 1041–1083.
Templado, J., Richter, A., Calvo, M., 2016. Reef building Mediterranean vermetid gastropods: disentangling the Dendropoma petraeum species complex. Mediterr. Mar. Sci. 17 (1), 13–31.
Trenhaile, A.S., 2015. Coastal notches: Their morphology, formation, and function. Earth Sci. Rev. 150, 285–304.
Vacchi, M., Marriner, N., Morhange, C., Spada, G., Fontana, A., Rovere, A., 2016. Multiproxy assessment of Holocene relative sea-level changes in the western Mediterranean: sea-level variability and improvements in the definition of the isostatic signal. Earth Sci. Rev. 155, 172–197.
Van Alfen, P.G., 1996. New light on the 7th-c. Yassi Ada shipwreck: capacities and standard sizes of LRA1 amphoras. J. Roman Archaeol. 9, 189–213.
Vousdoukas, M.I., Velegrakis, A.F., Plomaritis, T.A., 2007. Beachrock occurrence, characteristics, formation mechanisms and impacts. Earth Sci. Rev. 85 (1–2), 23–46.
Whitehouse, P.L., 2018. Glacial isostatic adjustment modelling: historical perspectives, recent advances, and future directions. Earth Surf. Dynamics 6 (2), 401–429.
Yokoyama, Y., Lambeck, K., De Deckker, P., Johnston, P., Fifield, L.K., 2000. Timing of the Last Glacial Maximum from observed sea-level minima. Nature 406 (6797), 713–716.